FINAL PUBLISHABLE REPORT

Grant Agreement number	17IND03
Project short name	LaVA
Project full title	Large Volume Metrology Applications

Project start date and duration:		1 August 2018, 45 months
Coordinator: Andrew Lewis, NPL Tel: +44 208943 6074 E-mail: andrew.lewis@npl.co.uk Project website address: http://empir.npl.co.uk/lava/		
Internal Funded Partners: 1. NPL, UK 2. CNAM, FR 3. GUM, PL 4. INRIM, IT 5. LNE, FR 6. RISE, SE 7. VTT, FI	External Funded Partners: 8. FID, IT 9. TEKNIKER, ES 10. ISI, CZ 11. RWTH, DE	Unfunded Partners: 12.MAPVISION, FI (withdrawn 31 January 2020) 13.SAAB, SE
RMG: -		

This publication reflects only the author's view and the Commission is not responsible for any use that may be made of the information it contains.

The EMPIR initiative is co-funded by the European Union's Horizon 2020 research and innovation programme and the EMPIR Participating States

TABLE OF CONTENTS

1 Overview

This project targeted improved, accurate, traceable measuring systems for operation as Large Volume Metrology (LVM) tools and integration of these tools into a factory coordinate metrology network. The network and tools were designed and built to be suitable for operation in typical factory environments or for permanent inclusion inside manufacturing systems such as large machine tools, industrial robots, *etc*., in accordance with ISO Geometrical Product Specification (GPS) standards. The new tools and technologies offer better accuracy than existing systems, enhanced uncertainty calculation and budgeting, improved compensation methods for air refractive index, and the ability to interface with production and assembly process control, resulting in traceability, efficiency and cost improvements in industries & science facilities relying on LVM.

2 Need

LVM is often hidden from consumers but is vital for the manufacture and alignment of many items upon which modern life and leading-edge science depend. LVM is necessary because the item or items to be measured or aligned are too large to fit within conventional measuring machines or too bulky to transport to a calibration laboratory – they must be measured *in situ*, often in non-cooperative environments. Aviation, the biggest sector user of LVM, needs to deliver new, lighter aircraft but the metrology tools to achieve the smaller tolerances on large parts do not exist. Existing industrial factories *e.g.* automotive, inspect only ~1 % of items and do this offline as inline tools are slow and not traceable, leading to inefficiency. Industry 4.0 and Digital Factories presuppose that Automatic Guided Vehicles (AGVs) and robotics in factories can achieve necessary positioning and alignment accuracies with real-time control but this is far from being available. The *Institute For Robotics* and *IEEE Robotics and Automation Society* have stated that real-time feedback is a fundamental requirement for *e.g.* robotic drilling machines where accurate metrology over large volumes is needed, but this is not yet delivered commercially (typical robot: 0.5 mm accuracy, typical required tolerances: 0.1 mm). Large volume factory metrology networks are not sufficiently accurate and local solutions based on laser trackers are too expensive or too slow and there is no integration between localised metrology and factory-wide metrology, impeding the in-process transition between different metrology devices. Up to now, existing LVM tools (*e.g*. laser trackers, laser radar) have used single point refractive index compensation, therefore fail to deliver claimed accuracies in real-world factories where temperature gradients exist or change quickly. Large machine tools must be error mapped ('calibrated') to achieve specification but this is expensive, time-consuming and undertaken only occasionally, leading to accuracy or downtime issues. There have been demands for additional novel LVM tools based on novel and/or cheap sensors and techniques for the ever-expanding range of end user scenarios *e.g.* higher accuracy (cheap) photogrammetry, and absolute distance 3D coordinates at long ranges, useable in harsh environments. Additionally, there has been a need for novel systems to bridge the gap between expensive but accurate laser trackers and cheaper but less accurate photogrammetry.

3 Objectives

The project aimed to deliver a range of improved and/or novel LVM systems, capable of *in situ* operation in factory environments, and to network several of these systems together to provide the metrology infrastructure for a digitally-enabled Future Factory demonstrator. To achieve this the specific objectives were:

1. To improve the metrology capability of Frequency Scanning Interferometry (FSI)-based techniques beyond the state-of-the-art by removing the current accuracy limitation of the necessary gas cell frequency standard through improved spectroscopy.
2. To develop novel and validated LVM methods for simultaneous metrology of multiple items at different scales and accuracies including: (i) close range precision tracking of robotic systems, (ii) medium accuracy 3D positioning within whole factory volumes and adjustable accuracy tracking for Autonomously Guided Vehicles carrying workpieces.
3. To develop and demonstrate techniques for *in situ* high accuracy (~10^{-7}) air refractive index determination with factory-sized volumes.

4. To develop models to simulate self-organising production and assembly based on digital information from process-integrated measurement systems and to apply these methods to other project outputs to produce an industrial scenario demonstrator.
5. To produce equipment and validated methods for evaluating the performance and compensating for the errors of large machine tools (> 50 m³); the cost and operability must be adequate to leave the equipment on board or on the shop floor.
6. To facilitate the take up of the technology and measurement infrastructure developed in the project by the measurement supply chain, standards developing organisations *e.g.* ISO/TC 213, and end users *e.g.* the automotive and aerospace industry, through operation of one or more demonstration activities, in addition to publications, training, and stakeholder interaction.

4 Results

4.1 Improving the metrology capability of Frequency Scanning Interferometry (FSI)-based techniques beyond the state-of-the-art by removing the current accuracy limitation of the necessary gas cell frequency standard through improved spectroscopy.

Frequency Scanning Interferometry (FSI) is a powerful technique that can measure absolute distances. It is often used as a 'rangefinder' system to determine the range between a measuring device and one or more reflecting targets (or semi-reflecting surfaces, *e.g.* walls). One may already be familiar with the laser range-finders (often referred to as 'laser distos' within the surveying community) which can be purchased for a few hundred Euros. These devices take a fraction of a second to determine the range to a target (often a surface such as a wall) and they are often used by surveyors in measuring properties for sale. The accuracy achievable is of the order of 1 mm to 2 mm which is sufficient for their intended purpose, but insufficient for manufacturing metrology. An extension of the concept has been used by several researchers to produce a much more accurate rangefinder, for example the work by NPL in the LUMINAR project [EMRP project IND32, http://projects.npl.co.uk/luminar/]. Here, a laser is scanned over a range of wavelengths (optical frequencies) with the output of the laser coupled into one or more interferometers. As the laser is scanned, the detector in each interferometer observes a pseudo-sinusoidal variation in intensity caused by the changing wavelength of the laser compared with the fixed distance to the target. Analysis of the interference signal can be used to find the distance from the interferometer to the target. By scanning over a large enough range of wavelengths the range of the technique can be extended to several tens of metres, and by knowing the exact wavelength variation during the scan, the accuracy can be improved. Accuracies of the order of tens of micrometres are possible. Such systems are highly attractive to users such as the aerospace industry where large items (tens of metres) need to be assembled or monitored. Currently laser trackers are the most popular high accuracy large volume metrology tool, but these are only single target devices, *i.e.* they track or measure the distance to one target at a time. Tracking multiple targets simultaneously is only possible by buying more laser trackers (essentially one per parget).

Advanced multi-beam FSI systems (*e.g*. the NPL system from LUMINAR) can handle multiple targets simultaneously. The scanning lasers used in these systems perform their scan independently of any reference – the speed of the scan and the exact start and end values of the wavelength are not guaranteed. A way to solve this problem is to send part of the laser light into a gas cell containing a gas with quantum absorption features within the wavelength range of the scanning laser. By monitoring the light transmitted through the cell, the system can detect these absorption features (periodic dips in the transmitted signal). Each feature corresponds to a precise wavelength value with the values determined by the quantum transitions in the gas species, *i.e.* they are standardized. As each feature is passed during the scan, it serves as a wavelength (or frequency) reference, enabling the system to know both the wavelength at that moment, and also the speed of the scan (by comparing the times when two different features are detected). If the frequencies of these features are pre-measured using techniques traceable to the SI metre or SI second, the features can serve as traceability references for the scanning laser – *i.e*. the system becomes SI traceable.

Similar sets of transition features have been used for decades to provide frequency references for ultra-stable lasers, with perhaps the most-used such system being the helium-neon laser at 633 nm (the well-known red

laser wavelength) locked to transitions in the iodine molecule. Such iodine-stabilized He-Ne lasers are used at many laboratories as the national realization of the SI metre. The frequencies of the iodine transitions have been measured with high accuracy by several researchers and the international community has agreed on the values of these transitions and their uncertainties. Unfortunately, the situation is not so ideal for the wavelength range used by common frequency scanning infra-red lasers such as those used in the NPL system. The wavelength range of interest is 1540 nm to 1560 nm and there are only a few known gas species in this range with absorption features: acetylene and hydrogen cyanide (HCN). The acetylene values are well-known with high accuracy and internationally agreed values [https://www.bipm.org/documents/20126/41590985/M-e-P_13C2H2_1.54.pdf/623e90e2-e816-36f7-2fd3-93b2e741ee5c] however they are not well-positioned in the wavelength range of typical scanning lasers (only covering 1510 nm to 1540 nm). Better placed are the HCN transitions (covering 1530 nm to 1560 nm), however these only have one moderately accurate set of data from 1998 [https://nvlpubs.nist.gov/nistpubs/Legacy/SP/nistspecialpublication260-137.pdf].

This data (from NIST), reproduced in figure 1 for reference, claims an expanded uncertainty on each wavelength value of 0.003 nm, *e.g.* 1528.054 nm ±0.003 nm for the R-25 feature. This means the fractional uncertainty is 2 parts per million. If used as a frequency (wavelength) reference in an FSI-based rangefinder, this would be a 2 µm uncertainty for each 1 m rage. Over typical large ranges, *e.g.* 20 m, this would amount to a 40 µm uncertainty which is too large. There are three additional issues. Firstly, the correction due to the pressure of the gas in the cell was determined by the NIST researchers, but with relatively poor accuracy (meaning that correcting for the pressure in each cell becomes the limiting uncertainty). Secondly, due to the moderately low accuracies of the values in the NIST publication, the HCN spectrum has not been internationally ratified as a frequency (wavelength) standard, *i.e.* it Is not SI-traceable. Thirdly, recent work by researchers using the HCN transitions as frequency references has identified a possible correlated uncertainty (*i.e.* an error) in the values published by NIST (possibly as high as 300 kHz) [https://doi.org/10.1364/OE.22.024869].

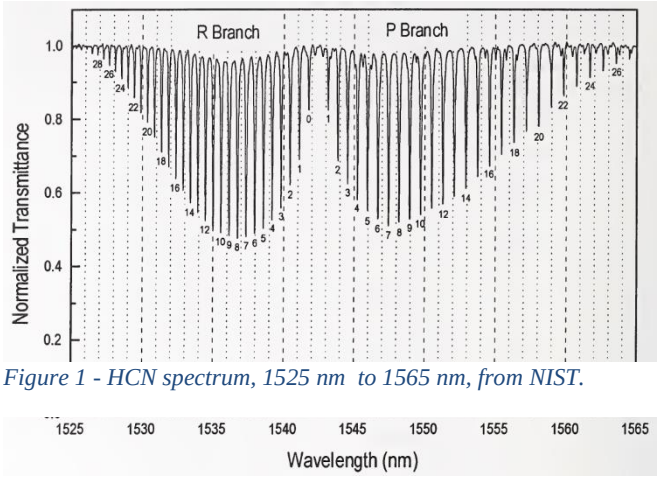

Figure 1 - HCN spectrum, 1525 nm to 1565 nm, from NIST.

The wavelength range used in the FSI system is also of interest to the telecoms industry (hence the availability of lasers operating in this region). With all these requirements in mind, Objective 1 of the LaVA project was centered around deriving higher accuracy values for the HCN absorption spectrum and making these internationally ratified. The project tackled this need by having three partners attempt independent measurement of the HCN spectrum using different techniques, followed by publication of their results prior to consideration by the international community as an agreed frequency reference. The three partners involved in the work were: NPL – using a dual frequency comb technique; ISI – who tackled both linear and saturated absorption spectroscopy using frequency locked lasers; and RISE- who used Fourier Transform Infrared Spectroscopy. The workflow was for each partner to independently prepare their measurement setup, measure the relevant features (ideally at different pressures and temperatures in order to derive the pressure- and temperature-sensitivity coefficients), to publish the data in open access peer reviewed publications, and then request the Working Group on Frequency Standards, CCL-CCTF-WGFS (a joint Working Group of the CIPM Consultative Committees for Length and for Time and Frequency) to ratify the data and accept it into the list of *Recommended values of standard frequencies* which is published by the BIPM [https://www.bipm.org/en/publications/mises-en-pratique/standard-frequencies].

ISI followed two broad approaches to the work, firstly using linear spectroscopy with its relatively simple experimental setup, followed by saturated absorption spectroscopy which is more complex but offers the finest resolution. A first test setup, to obtain familiarity with the HCN gas was prepared, first using well-known acetylene gas (in a cell at 100 Pa pressure) instead of HCN. An available tuneable laser with a relatively narrow tuning range (1539.8 nm to 1541.0 nm) was used together with an optical frequency comb and laser stabilization optics. The light from the laser was used to beat against the comb in order to obtain a precise frequency reference. The laser was first fast tuned over its range to observe which lines were visible, followed by slow tuning to obtain line profiles and eventually locking to each line centre to obtain the most accurate line centre frequency. After tests with the acetylene gas, the HCN gas was investigated. The system was found to cover three lines of the acetylene spectrum – P(12), P(18) and P(13). The line centres were measured, and the results compared well with the reference data for this gas. The HCN gas cell was substituted for the acetylene

cell and a fast frequency scan revealed the presence of one HCN feature – the R(s) line. Slow scanning of the line followed by frequency locking to the line centre obtained results with an uncertainty of ~10^{-8}, which was already more accurate than the previous reference data. The early investigative work from ISI was published:

> "Investigating The Use Of The Hydrogen Cyanide (HCN) As An Absorption Media For Laser Spectroscopy", M. Hošek *et al*., *Proc. SPIE* **Vol. 10976** 1097601-1 (2018) DOI:10.1117/12.2517761 with an open access version of the work available here: https://arxiv.org/abs/1905.07272

In this initial experiment, the tuning range of the laser was insufficient to access other features and so a new system had to be designed around a new laser source. A new continuously tuneable laser covering 1510 nm to 1630 nm was obtained. As before, the frequency reference for beat note frequency measurements came from an optical frequency comb which derived its primary frequency reference at 10 MHz from a hydrogen maser. The gas cell was housed inside a temperature controlled chamber to hold the temperature (and pressure) of the gas constant during measurement. Frequency modulation at 10 kHz and 6 MHz depth was used in the lock-in amplifier, with this modulation being removed in the detection electronics. One by one, the system was tuned to each accessible feature, and locked to the line centre for ~8 hours. Data from these locked periods was analysed to check for stability – the results showed very good Normal distributions with 2-sigma variance or around 40 kHz and Allan deviations minima of around 10^{-10}, showing excellent frequency stability of the locked laser. All the lines were found to be about 400 MHz broadened by Doppler broadening which can only be removed using saturated absorption spectroscopy (which was the next stage of the work). The detailed ISI linear spectroscopy work was published:

> "Measurement of the Hydrogen Cyanide Absorption Lines' Centers with the Potential for Mise en Pratique", M. Hošek, *et al*., published in *Proc. IEEE*, (2021), ISBN 978-1-6654-3935-0, 7189, DOI:10.1109/EFTF/IFCS52194.2021.9604261 with an open access version of the work available here: https://zenodo.org/record/6497486

The updated HCN values from the detailed ISI linear spectroscopy publication are reproduced in the table below; they cover both the so-called P- and R-branches of the $2\nu_3$ rotational-vibrational band of $H^{13}C^{14}N$. At the time of preparing this report (*i.e.* before the final papers from IS are published) these represent the state-of-the-art knowledge of the HCN spectrum in this wavelength (frequency) range, surpassing the previous reference data published by NIST.

R branch	*f*/MHz	*u*/MHz		P branch	*f*/MHz	*u*/MHz
2	194,615,893.43	0.06		3	194,101,383.63	0.06
3	194,697,533.81	0.06		4	194,011,539.87	0.05
4	194,777,994.36	0.04		5	193,920,532.34	0.04
5	194,857,273.35	0.04		6	193,828,363.34	0.05
6	194,935,369.49	0.04		7	193,735,034.34	0.04
7	195,012,280.18	0.04		8	193,640,548.56	0.04
8	195,088,004.33	0.04		9	193,544,907.37	0.04
9	195,162,540.03	0.05		10	193,448,113.37	0.05
10	195,235,885.62	0.05		11	193,350,168.82	0.04
11	195,308,039.52	0.05		12	193,251,076.07	0.04
12	195,379,000.21	0.05		13	193,150,838.24	0.05
13	195,448,766.29	0.04		14	193,049,454.45	0.06
14	195,517,335.80	0.05		15	192,946,931.25	0.07

Table 1 - linear spectroscopy of HCN - results from ISI.

Although the data published in this linear spectroscopy paper is sufficient for the project objective on improving FSI accuracy, the possibility of using HCN as a high precision frequency reference for the metre realisation (or for telecommunications work) meant that the more accurate available from the more complex, saturated absorption spectroscopy approach would be useful and help convince the WGFS to ratify the data at higher accuracy level. ISI thus changed experimental setup to allow saturated absorption spectroscopy to be performed.

A classical setup using counter-propagating beams in a gas cell at 50 Pa was constructed with the gas cell permanently attached to a vacuum manifold to allow refilling at different pressures. A single frequency erbium-doped low noise laser was amplified by an erbium-doped fibre amplifier. The amplified light was split between the beams interacting in the gas cell, and a separate fibre-based HCN cell which was used for course frequency reference during laser tuning using the previously measured linear absorption spectrum. The laser frequency

was modulated at 1 kHz with 6 MHz depth and demodulated in the detection electronics. The optimum gas cell pressure was found to be ~2.5 Pa where a signal to noise ratio of ~100 was obtained. ISI then had to overcome a problem in which the signal level decayed by 50 % in 45 minutes. This is thought to be due to absorption of the polarised HCN molecule onto the cell wall, starving the beams of molecular interaction. ISI found that pre-coating the cell wall with silane (SiH_4) could reduce the decay to 50 % signal drop in 90 hours. Work on improving this situation is ongoing, however ISI were able to obtain a good 3*f* saturated absorption signal of the R(2) HCN line indicating that saturated absorption spectroscopic measurements should be possible, given more time. An initial paper on the ISI saturated absorption spectroscopy was published:

> "Saturated Spectroscopy of HCN", Jan Hrabina, Martin Hošek, Šimon Řeřucha, Lenka Pravdová, Josef Lazar; Ondřej Číp, Zdeněk Pilát, Proceedings of 2021 Joint Conference of the European Frequency and Time Forum and IEEE International Frequency Control Symposium (EFTF/IFCS), *Proc. IEEE*, 2021, (2021), ISBN 978-1-6654-3935-0, 7154. https://doi.org/10.1109/EFTF/IFCS52194.2021.9604272 Open access version of the work is available here: https://zenodo.org/record/6497501

ISI's work on the saturated absorption spectroscopy continued to the end of the project and two further publications are to be submitted shortly after the end of the project (in addition to the contracted deliverable which is already published). One paper will be a further paper on the linear spectroscopy. The other is a more detailed paper on the results of the saturated absorption spectroscopy - this paper was submitted for publication during the end of project reporting period, to the journal *Optics Letters*. We hope to report a DOI of an accepted publication at a later date (to the EURAMET repository and the project website), but until then, the preprint is available from ArXiv: https://doi.org/10.48550/arXiv.2206.09232.

The second partner to attempt HCN spectroscopy was NPL, and their approach was to use the technique of dual optical frequency comb spectroscopy in which two optical frequency combs are operated at slightly different repetition rates. A continuous wave laser at ~1.5 µm is split into two beams, one per comb, and the combs use perturbation (at slightly different frequencies) to produce modes ('comb teeth') at regular spacings, with traceability to the H-maser frequency reference. The two combs with repetition rates f_r and f_r+Δf_r are mixed and detected by a single photoreceiver. Each pair of optical teeth (one from each comb) yields an RF heterodyne signal at an RF frequency. These RF frequencies form a comb in the RF domain of spacing Δf_r. The spacing between the RF teeth can therefore be adjusted by changing Δf_r. For spectroscopy, either one or both combs are passed through the sample gas. The resulting absorption (or phase shift) visible on the optical domain comb teeth is encoded onto the corresponding amplitude (or phase) of the measured comb teeth in the RF domain. Because the RF signal is low enough in frequency for direct detection, it serves as a measurable proxy for the optical signal. The dual comb system maps the optical spectrum of width, $\Delta\nu$, to an RF spectrum of width, $\Delta\nu/m$, where $m=f_r/\Delta f_r$. Normalization of the RF signal is performed using a beam which does not pass through the gas sample. The optical scheme is shown in Figure 2 together with the equipment setup in the NPL lab.

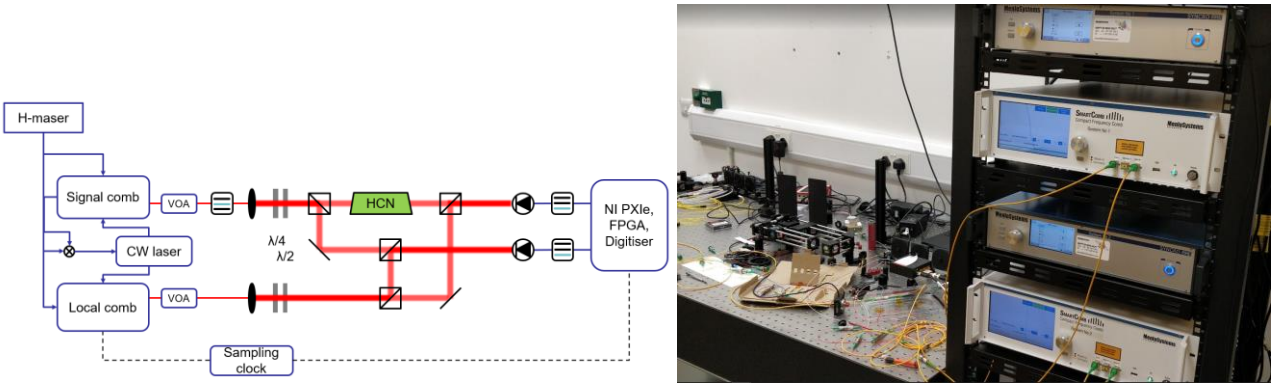

Figure 2 - left: optical scheme of the NPL comb system; right: photo of the HCN spectroscopy lab.

The two combs use repetition rate synchronization electronics which are linked to NPL's hydrogen maser frequency reference in order to ensure the two combs are fully referenced to one another ensuring mutual coherence and high signal to noise ratio (SNR). A single absorption spectrum can be obtained during a single sweep of the laser (*i.e.* every $1/f_r$) but for improved SNR, multiple sweeps (interferograms) need to be acquired and averaged, necessitating high speed synchronized data acquisition to allow for phase correction. As well as being prepared for free space optics, initial tests were performed using fibre-coupled gas cells.

Unfortunately, the COVID-19 pandemic caused a long delay in preparing the NPL experimental system as the frequency combs were ordered rather late (due to COVID-19 shutdown) and delivery was then delayed further. Additional problems with some components of the system caused further delays. Separately, the changing landscape caused by COVID-19 meant that all three of the NPL comb researchers resigned and left NPL before the end of the project and NPL was unable to resource the work to completion. In the end, with the delayed experimental setup and loss of key staff, the NPL experiment was unable to produce data suitable for publication within the timeframe of the project. The comb system remains at NPL, and it is hoped to be able to continue work after the end of the project, using alternative funds.

At RISE, an analysis of the unsaturated absorption spectra of HCN was performed in collaboration with Thorlabs Scandinavia. A fiber coupled gas cell with HCN at 100 torr and a path length of 5.5 cm was connected to an incoherent light source and the Fourier Transform Optical Spectrum Analyzer “Redstone OSA 305”. The analyzer uses a scanning Michelson interferometer with a frequency-locked 1532.8323 nm reference laser. To further reduce uncertainties of spectral offset caused by alignment of input light, the HCN gas cell under test is connected in series with an Acetylene gas cell. Thus, any frequency error will be corrected with the offset of the H_2C_2 absorptions as specified in the Mise en Pratique. Also, this indicates that traceability will be achieved through the official absorption frequencies of Acetylene. The sample resolution of the Spectrum Analyzer is 2.0 GHz, but this can be improved through curve fitting algorithms. The analysis of the total measurement uncertainty is ongoing, and the results are planned to be submitted for publication in the IOP journal *Measurement Science and Technology*.

At the end of the project, ISI had published three papers, including the paper where they listed the improved HCN frequency data given above. This alone should be sufficient for consideration by the CCL-CCTF WGFS. However this is not the only output – the work by RISE is also to be published and two further papers by ISI will be published after the end of the project; the papers will be submitted to the CCL-CCTF-WGFS as additional data to the main publication by ISI. The CCL-CCTF-WGFS is expected to meet next in autumn 2022 and NPL will table the formal request to the WG to review the new HCN data with a view to incorporation into the List of Recommended values of Standard Frequencies. As such, the project has delivered what was required to fulfil objective 1.

As confirmation of the timely need for this improved HCN data, NPL has been asked to supply two fully operational FSI systems (the OPTIMUM system) to advanced manufacturing research organizations – the Advanced Manufacturing Research Centre (AMCR) in Wales [https://www.amrc.co.uk/facilities/amrc-cymru-wales] (which is partnered by Boeing) and the Advanced Machinery and Productivity Institute [https://www.ampi.org.uk/] (AMPI). Both systems will be using the updated HCN data to provide the FSI traceability route.

4.2 Development of novel and validated LVM methods for simultaneous metrology of multiple items at different scales and accuracies including: (i) close range precision tracking of robotic systems, (ii) medium accuracy 3D positioning within whole factory volumes and adjustable accuracy tracking for Autonomously Guided Vehicles (AGV) carrying workpieces.

Within advanced manufacturing, a key trend is towards automated and eventually autonomous production, with a strong emphasis on robotics and robotic-assisted manufacturing and assembly. However many robotic systems lack sufficient accuracy for fully autonomous operation and several project partners have therefore developed coordinate metrology systems to track manufacturing robots and AGVs. As these devices operate over several distance scales (from close-range operations and inspection to entire factory part positioning), the developed metrology solutions also need to cover several scales. This has necessitated research into building several metrology systems, operating on different principles and at different scales.

LNE photogrammetry system

A close range photogrammetry system (3D scanner) has been designed, manufactured and assembled by LNE (see Figure 3) to control the geometrical quality of large mechanical parts, including both form errors and areal surface texture. The developed 3D scanner (a) consists of two monochrome industrial cameras (h) (Ximea MQ013rg-e2 equipped with digital lens LM8JCM-V of 8.5mm focal length) and one structured lighting projector (i) (DLP Lightcrafter 4500). Each camera is fixed on a horizontal rotational structure (f) to guarantee a predefined overlapping between both cameras FoVs. The structured lighting projector is fixed on one additional vertical rotational structure (g) to align the projected fringes with the cameras FoVs. Furthermore, the rotational structures allow the adoption of several angular configurations of the monochrome industrial cameras and projector, consequently several overlapping values could be fixed. The rigid frame (j) made of aluminium material supports the cameras-projector assembly. The 3D scanner is mounted on the end-effector of the KAWAZAKI industrial robot (d), with a maximum reach of 620 mm and positioning repeatability of 20 µm.

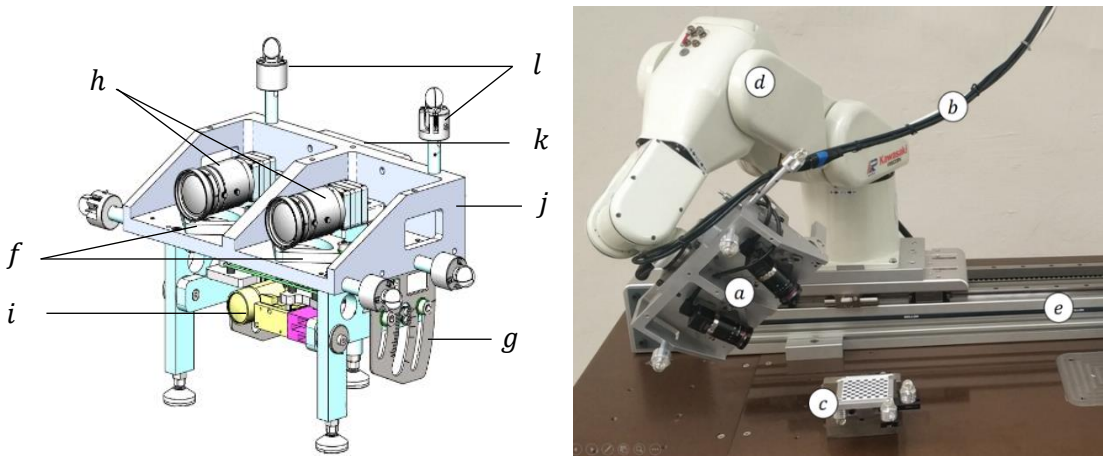

Figure 3 - the LNE-developed close range photogrammetry system: (a) 3D scanning system; (b) Connection cables to the ter-minal computer; (c) Checkerboard calibration grid; (d) Industrial 6-axis KAWASAKI robot; (e) 7th motion axis; (f) Camera mounting brackets; (g) Projector angular positioning; (h) Monochrome industrial cameras (i) Industrial projector; (j) Aluminium mounting system; (k) Scanner-robot fixing part; (l) Spheres for laser rangefinders.

Traceability of the system was achieved through the use of target grids which had been calibrated using optical CMMs. The camera calibration and solution of the photogrammetry network involved particle-swarm approaches. To demonstrate the integration of the LNE system in a wide factory network (simulating the repositioning of the system via some form of large robot, within the factory volume), a multilateration system developed by CNAM was used to track the LNE robotic photogrammetry system, with uncertainties of the order of a few micrometres.

The system developed by LNE thus delivers the metrology requirements of part (i) of this objective of the project, namely close range precision tracking of robotic systems and the combination with the CNAM system (reported elsewhere in this document) tackles part (ii) of the objective.

CNAM multilateration coordinate measurement system

The majority of the research by CNAM in the LaVA project concerned the development, testing and verification of their reference class three-dimensional coordinate measurement system based on absolute distance metrology. The aim was to develop a system that is more accurate than commercial laser trackers and can be considered as a metrological system, *i.e.* has traceability to the SI metre, including detailed assessment of the uncertainty of each measurement. For comparison, commercial laser trackers generally operate to a few tens of metres range and have a manufacturer specified Maximum Permissible Error (MPE) of 10 µm + 5 µm/m, but this can be exceeded in poor environments. As such, the CNAM system can deliver part (i) of the objective as well as part (ii), in the sense that it easily delivers the position accuracy at large ranges, though is designed for static targets rather than dynamic ones, especially when operating with corner cube targets. The system can deliver the base accuracy for a network of static targets which are then the references for dynamic systems.

The system is based around 4 'measuring heads' which point optical beams at a target in order to measure the distance between a reference point in the head and the target. The positions of the heads are initially unknown and determined by a multilateration algorithm with self-calibration: when a sufficient number of targets is measured, a system with more equations than unknowns is obtained. It is then possible to determine the coordinates of the 4 heads and of the targets (with a global offset).

The measuring heads use an absolute distance meter (ADM). The ADM determines the distances *d* between each measurement head and a target position. To do this, a phasemeter measures the phase accumulated by a Radio Frequency (RF) carrier, which is propagated in air by a laser beam at 1550 nm:

$$d = \frac{1}{2} \times \left(\frac{\phi}{2\pi} + k\right) \times \frac{c}{n \times f_{RF}} \#(1)$$

Here ϕ is the measured phase shift, c the speed of light in vacuum, n the group refractive index of air, f_{RF} the frequency modulation, and k an integer number corresponding to the number of synthetic wavelengths $\Lambda = c / (n \times f_{RF})$ within the distance to be measured. The ADM uses affordable components coming from the telecommunications industry: the emitted modulated signal comes from a Distributed FeedBack laser diode (DFB) modulated at 4895 MHz by an Electro-Absorption Modulator (EAM), while at the receiver side, the phase-shifted signal is detected by a PIN photodiode. To reduce the cost of the system, a common ADM is shared between the four measuring heads using a fibre switch, thus with the developed system, the four distance measurements for a given target are not measured simultaneously, but one after the other (time multiplexing).

The measuring heads employ dual axis gimbal systems to control the pointing direction of each head and each head features a modified mounting carrier (original component manufactured by Leica) to allow mounting onto a wide range of existing surveying hardware. An assessment of the mechanical errors of the system is presented in a journal paper in *Rev. Sci. Instrum*: https://doi.org/10.1063/1.5132933

The multilateration system can be used with two kinds of retroreflector, a hollow corner cube or a glass sphere. The hollow corner cube is suitable for long-distance measurements, up to 140 m, while the sphere, which induces high optical losses due to bad reflectivity and beam deflection at its output, is preferred for short distances up to 20 m since it offers a visibility from any angle, a light weight, and a more competitive price. The hollow reflector is mounted in a steering system as it has a limited acceptance angle across the front face and has to turn to face each measurement head (whilst keeping the optical centre fixed in space).

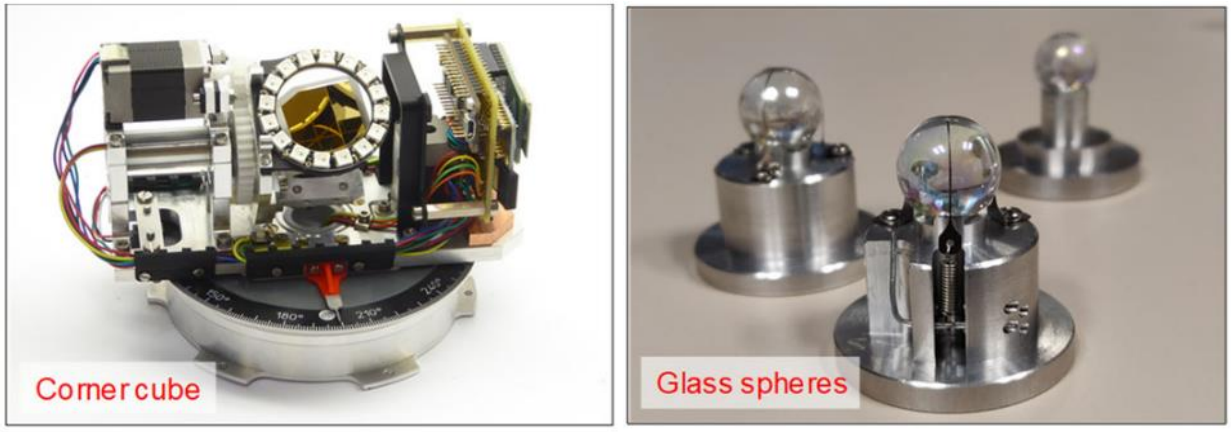

Figure 4 - the two type of reflector used in the CNAM system: left - hollow corner cube in motorised stage; right - glass spheres.

Overall the measurement heads were found to be capable of delivering optical range measurement with an uncertainty better than 5 µm over path lengths up to 20 m, and the total standard uncertainty on distance measurement (including mechanical errors of the heads) is 11 µm which is state of the art. The heads are also capable of making measurements up to 140 m range (far greater than commercial laser trackers).

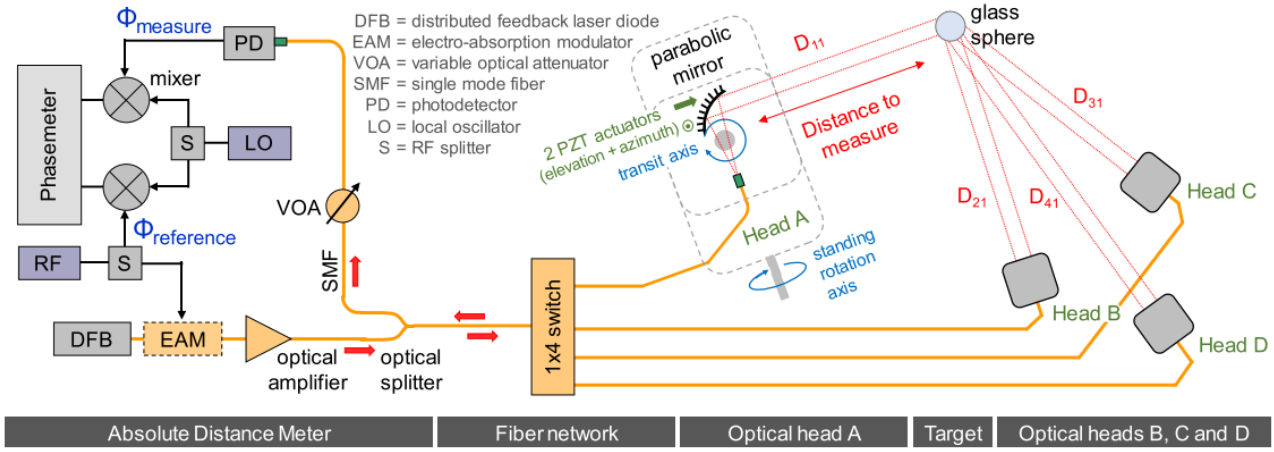

Figure 5 - schema of the CNAM multilateration measurement system.

By using the four measuring heads to measure the same common target, a multilateration-based coordinate measuring system is achieved. The metrological basis of the system is the determination of the distances from all four heads to the common target. After measurement, the target is moved to a new location and the distance measurements are repeated. When sufficient measurements have been completed, the system becomes mathematically solvable, revealing the 3D locations of the heads and the locations where the target was measured. The schema of such a system is shown in Figure 5.

However, the combination of range information from multiple heads into a multilateration-based coordinate measurement system can achieve an improvement on the 3D position uncertainty, especially if the locations of the measuring heads are chosen carefully. The reason for this is that the uncertainty field obtained by each head is in the form of an ellipsoid, with unequal axes. By arranging the heads such that the four ellipsoids (one from each head) are enmeshed in a way that distributes the ellipsoid axes equally in 3D, the combined uncertainty will be minimised as no two ellipsoids will have their major axes aligned. When the heads are positioned in one of the arrangements shown in Figure 6, the overall 3D uncertainty of the measured target is minimised to a value of $3/\sqrt{4}$ of the range measurement uncertainty. With a range uncertainty of 5 µm, such an arrangement can achieve 7.5 µm uncertainty.

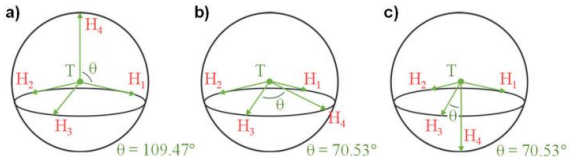

Figure 6 - optimum arrnagements of four multilateration heads and a target. a: regular tetrahedron; b: circularly-spaced tetrahedron; c: isosceles tetrahedron. These arrangements minimise the overall uncertainty ellipsoid size.

The details of the measuring heads and the overall multilateration system are described in a journal paper in *Precision Engineering* (https://doi.org/10.1016/j.precisioneng.2021.09.009).

The uncertainty of measurement obtained using a laser tracker can be difficult to calculate correctly as the commercial tracker software does not expose the underlying geometric model, nor its sensitivities, values or uncertainties. The model is further complicated by the mechanics of the laser tracker and the reliance on angle measurements in addition to the ranging. However, the CNAM measuring heads do not rely on the measurement of angles, and their mechanical model is known. This enables propagation of the relevant parameters into a GUM-compliant uncertainty calculation, taking into account factors such as uncertainty in the determination of the measurement head locations (through self-calibration multilateration). This means that a metrologically-compliant uncertainty of measurement can be obtained for every target location measured using the system. Together with the link to the SI unit realisations, the results of the system are fully SI traceable.

Figure 7 - photograph showing three of the four CNAM measuring heads as part of a multilateration network.

An initial assessment of the uncertainty of the system is described in the journal Precision Engineering: https://doi.org/10.1016/j.precisioneng.2020.08.002.

Verification of the uncertainty modelling was obtained through three experimental sets of measurements:

- a: a small volume of one cubic meter using a corner cube as target in 14 different positions; 3 triplet pairs of targets were constructed;
- b: a large volume with distances up to 11.5 m and a corner cube target in 14 different positions; the targets were arranged on 3 pillars and as 3 couples;
- c: a small volume of one cubic meter using a glass sphere of index n = 2 as target in 16 different positions; the targets were again arranged as 3 triplets.

The uncertainty on the measured distances (k = 1) has been assessed at 4.7 µm when the target is a corner cube and at 4.3 µm when it is a glass sphere of index n = 2. Reference measurements were obtained using the ADM aligned with the axis between each pair of target locations. In such a way, high accuracy inter-target

distances were obtained which formed the ground truth for the tests of the multilateration system. These distance measurements had an uncertainty of 7.1 µm. The differences between the inter-target distances (d1) (calculated from the multilateration data) and the directly measured distances (d3) are plotted in Figure 8.

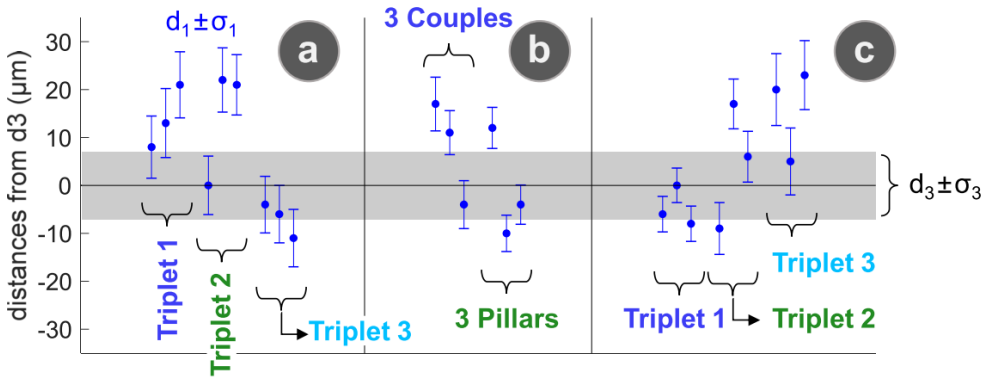

Figure 8 - results from comparison between multilateration-derived inter-target distances (d1) and the directly measured distances (d3). Uncertainty bars correspond to 68 % confidence level (k = 1).

The 68 % confidence level of accuracy that can be achieved with the developed system, when the arrangement of the heads is close to a regular tetrahedron, is typically between 6 µm and 10 µm for a small volume of one cubic meter and between 10 µm and 22 µm for a large volume with distance scale of the order of 5 m.

A further performance verification was obtained by comparison with measurement of a network of targets measured using a commercial laser tracker. Colleagues from RISE (Sweden) travelled to CNAM and used their Leica AT960-LR laser tracker. This comparison required a very careful assessment of the 3D error ellipsoids obtained by the four CNAM measuring heads as well as that of the laser tracker. Overall when looking at the deviations between the two instruments, 94 % of the measurements agreed on the target locations within their k = 2 uncertainties, as expected.

The results of the multilateration operation, a detailed assessment of the measurement uncertainty, and the comparison against a laser tracker are reported in a 2022 journal paper in *Metrology* (https://doi.org/10.3390/metrology2020015). In conclusion, with the advanced (yet affordable ADM) and the careful analysis of the uncertainty of the measuring heads and of the system as a whole, CNAM have demonstrated a 3D large range coordinate measuring system which achieves accuracies better than commercial instruments.

Large Volume Photogrammetry System / TEKNIKER

This system has been developed in WP2 Task 2.2: 3D position measuring system in large factories and has been previously named as system (ii-b) in the project description. The aim of this system is to measure the position of moving objects in a large factory with a demonstrated uncertainty.

One of the interests of this system is the assistance in the assembly of large parts; these complex assemblies require nowadays manual adjustment *via* trial and error or using large and complex rigs to assist the assembly. The second interest of this system is specifically targeting the tracking of AGVs. Recently AGVs have benefited from more advanced sensing technology and the implementation of Artificial Intelligence, delivering higher safety and more reliable navigation. However, typically the control system of an AGV is integrated in the vehicle itself, providing an autonomous working capability but not a full integration with the plant where it is working. TEKNIKER has provided a low-cost 3D position measuring system developed for the real-time 3D tracking of moving objects in large volumes such as factory shop floors. The technology employed for this solution is photogrammetry. Because this system is software-driven and uses off-the-shelf camera and computer components, it is easy and affordable to install, operate and repair. In addition, real-time position of the moving parts is measured automatically, without human intervention.

The selected approach to measure in real-time the position of items in factory shopfloors is based on the photogrammetry technique, making use of cameras and target points. As to the targets, near-infrared (NIR) LED lights have been selected as the most appropriate solution, because a NIR filter can be used in each camera lens to remove from the photograph most of the undesired environment light energy content. For this

purpose, battery-driven wireless active targets have been developed and manufactured. This makes the active and wireless infrared target solution the most interesting both from the point of view of implementation and robustness.

In the following two images it is shown the difference between working with the full light spectrum and using only a narrow bandwidth around the NIR wavelength used by the active targets. This test was performed at the beginning of the project in open air and under solar light, which is the most adverse condition, compared that of an indoor environment. In this preliminary test an incandescent halogen lamp was used (later 850 nm LEDs were adopted).

As can be seen, when filtering all the light wavelengths except for the 850 nm NIR light band, most of the undesired light energy content is eliminated, so the light emitted by the active target appears in front of a nearly black background excepting some minor unwanted reflections that can be filtered. Working in the NIR band therefore helps to identify the target in the scene.

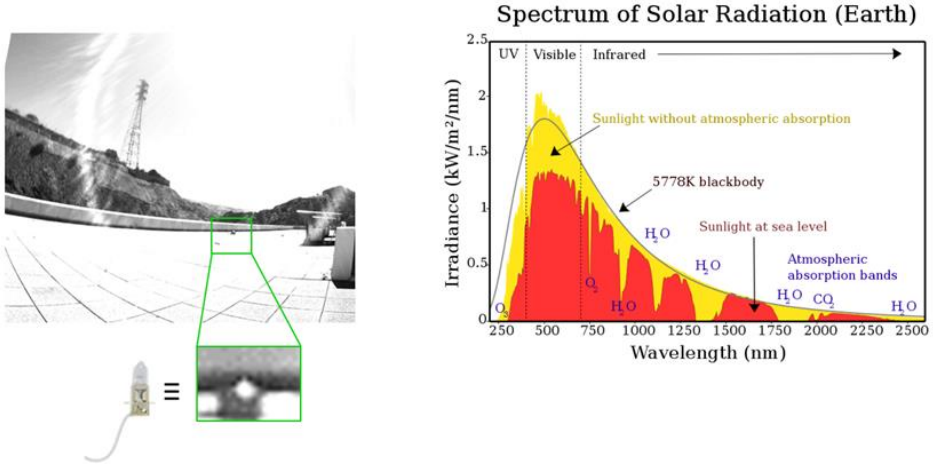

Figure 9 - testing of photogrammetry camera in sunlight without filtering.

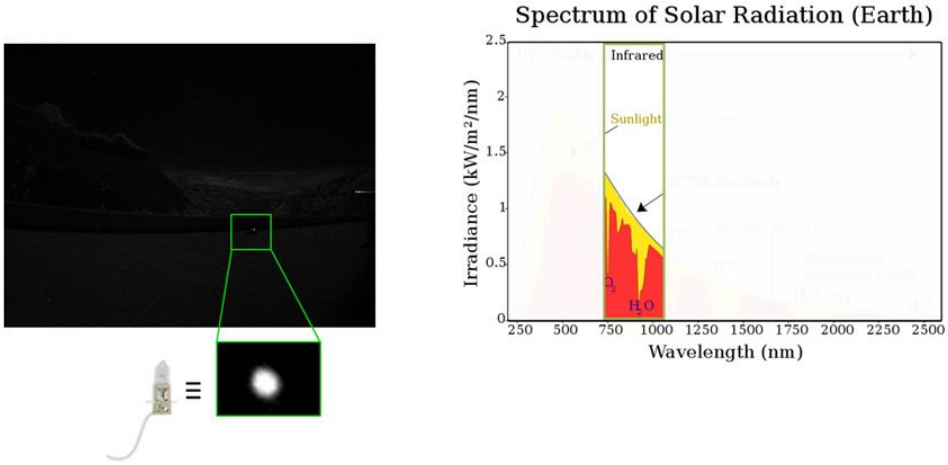

Figure 10 - testing of photogrammetry camera in sunlight but with filtering to exclude all but the NIR wavelength range.

The TEKNIKER-developed system can work with passive targets, but as explained earlier, working in the infrared spectrum band show an advantage for identifying the target in the scene.

There are two options for working in the NIR band. First is to use retro-reflective targets, which are illuminated by a set of several NIR light sources or lamps installed around the working volume of the system. The inconvenience of this approach is the buying cost of the lamps and the electricity expense derived of having the lamps continuously switched on.

In this project, a second approach has been embraced which is the use of self-powered battery driven active targets. For this purpose, the design and manufacture of 10 such active targets have been achieved. The

active targets have three 850 nm LEDs and a compact Lithium-ion battery cell with capacity to power the led intermittently for 8 hours which is the common working day duration.

The design of this system has included the electronics needed to handle the power management of the LED light source. Apart from the management of the battery and temperature control to prevent overheating, also the system has wireless communication capability. This is based on the use of a Bluetooth protocol and a remote control that allows to order the switching on and off from each single target from the main software installed in the computer.

Figure 11 - self-powered active targets developed by TEKNIKER.

Once the final cameras and lenses were selected, they were installed in a shopfloor, arranged in a volume of 10 m × 10 m × 5 m.

In the following images it is shown the kind of field of view that is obtained (these images are in the visible spectrum, although they will have later a filter to work in the infrared spectrum only).

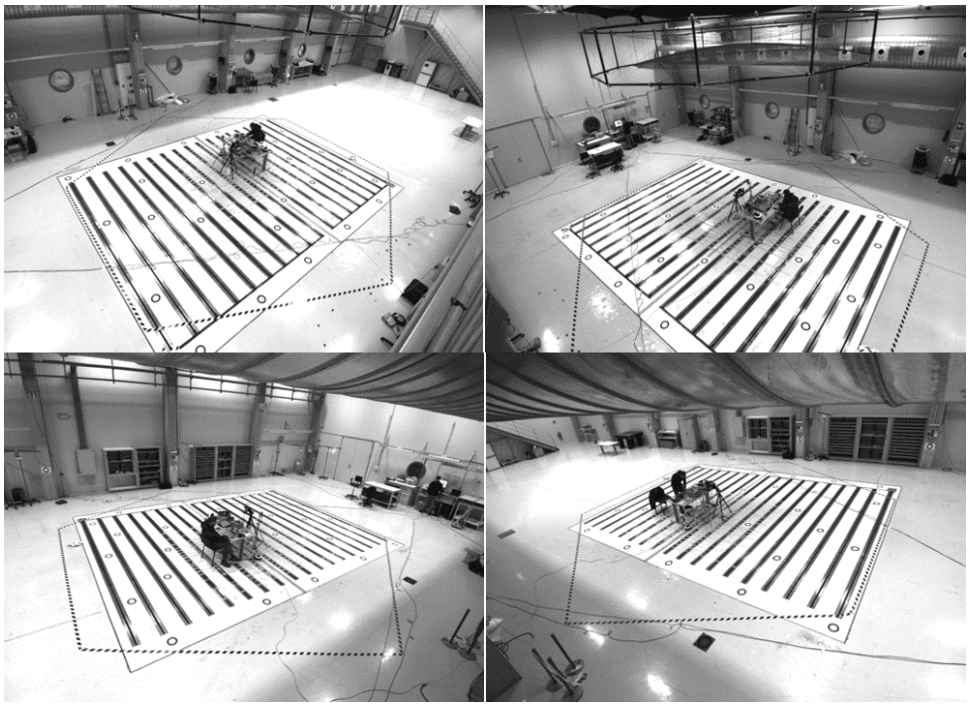

Figure 12 - images from the photogrammetry cameras covering the 10 m × 10 m × 5 m volume.

An automatic technique for *extrinsic* camera self-calibration was implemented to calculate the position and orientation of the cameras in the scene. This method, as shown in the next figure, has been based on a Bundle Adjustment algorithm which is used to estimate and refine both extrinsic camera parameters and 3D point

coordinates. This is an iterative method that aims to minimize the distances among observed image points and reprojected image points based on estimated model parameters. It can be used to solve the extrinsic orientation of multiple cameras and 3D points without *a priori* knowledge of these parameters.

Also, the absolute orientation corresponds to the coordinate system of the reference camera in this calibration method, thus it is necessary to transform this camera poses to the world coordinate system of the measuring system. Moreover, a scaling of the data is required as 3D points are also determined by the method but not scaled. One of advantages is that 3D point multi-view triangulation is also estimated at the same time, which enables one to measure a 3D scene with a camera network without knowing *a priori* where cameras are located and oriented in the scene.

To define both a scale, and also a traceability to the measurements, some reference targets were measured with a commercial Laser Tracker which had a certified metrological traceability. Once the extrinsic calibration has been done, only the triangulation of the measured points needs to be performed to achieve the results with a faster calculation.

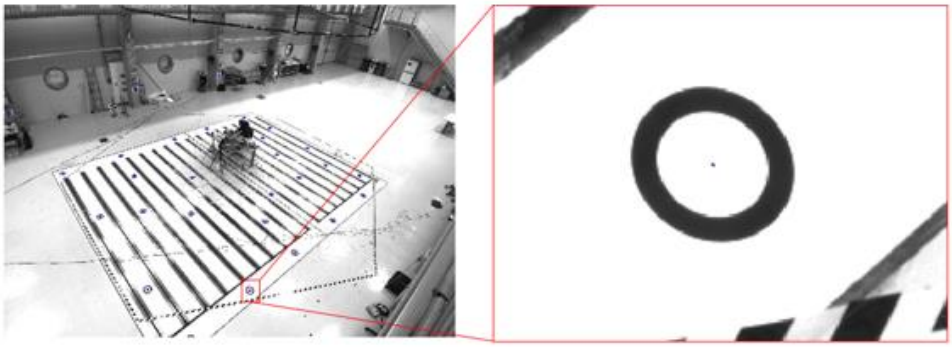

Figure 13 - reference targets, pre-measured using laser tracker.

Finally, a validation setup was prepared, consisting of an AGV moving in a real shopfloor environment, with an active target on top of the AGV. The position of the AGV was measured in real time using the photogrammetry system. Real time data was periodically uploaded to RWTH *via* the Unified Device Interface produced in WP4.

Figure 14 - AGV with active target.

Finally, a validation setup was prepared, consisting of an AGV moving in a real shopfloor environment, with an active target on top of the AGV. The position of the AGV was measured in real time using the photogrammetry system. Real time data was periodically uploaded to RWTH *via* the Unified Device Interface.

Traceability and accuracy for photogrammetry system / VTT-MAPVISION

Working with MAPVISION, VTT developed a calibration artefact comprising a carbon fiber shaft with well-defined targets. The targets are suitable for both tactile and optical probing, which allowed for calibration of all the target positions on the artefact with Coordinate Measuring Machine (CMM) at VTT, and then using the artefact inside the MAPVISION Quality Gate device in multiple orientations to perform a full calibration of the MAPVISION Quality Gate instrument. The artefact is 1400 mm long and the optical targets are made of white

machined Macor ceramic with molded black plastic centers. The eccentricity of the Macor outer circle and the central inner circle is 5 µm. The high modulus, low thermal expansion carbon fibre composite body is supported at the Bessel points. The optical contrast of the targets when measuring with the MAPVISION multi-camera system was found out to be good.

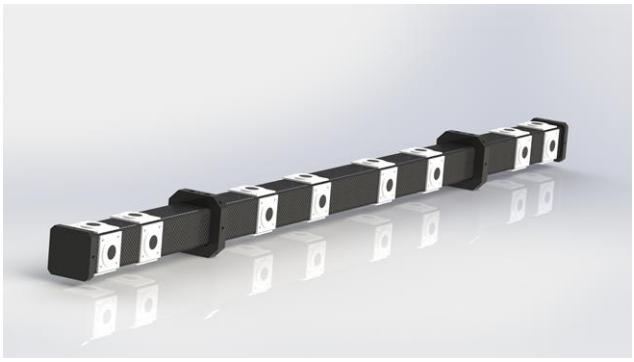

Figure 15 – the designed artefact for MAPVISION system calibration.

Figure 16 – the designed artefact inside a MAPVISION Quality Gate multi-camera chamber.

SAAB's contribution to this project objective was to act as a proxy stakeholder in preparation for some of the demonstrators and to supply a cargo door unit as a typical aerospace measurement artefact for one or more demonstrator scenarios. SAAB shared details of the cargo door demonstrator with the other project partners SAAB attended the relevant project meetings and plans were started for the distribution of the cargo door around the several demonstration activities. However, the COVID-19 pandemic caused cancellation of the demonstrators and the cargo door was not eventually used.

In summary, the project has delivered four novel systems which together, satisfy the objective of providing Novel/validated LVM methods for simultaneous metrology at different scales and accuracies. These are: the CNAM telemeter system, operating with 3.2 µm standard deviation up to 22 m range; the LNE dual camera photogrammetry surface scanning system, delivering 166 µm RMS error but much faster operation than a CMM (and operating over increased volume when coupled with the CNAM telemeter system); TEKNIKER's photogrammetry system, demonstrated over factory-sized volume with self-powered IR targets; and VTT's traceability route for photogrammetry, which is already being exploited by MAPVISION.

4.3 Development and demonstration of techniques for in situ high accuracy (~10^{-7}) air refractive index determination with factory-sized volumes.

The measurement of air refractive index is a critical part of many large volume measurement systems because the refractive index plays two key parts in the accuracy that can be obtained. Firstly, optical-based measuring systems which determine range to a target generally contain light of a known vacuum wavelength, but when the light is used in air, the wavelength is changed by the refractive index of the air - equivalently the speed of propagation is reduced by the air refractive index. Thus, the instrument has to measure or be informed of the refractive index to make a correction. For example, for air of standard gas concentration at standard atmospheric conditions (20 °C, 1013.25 hPa, 50 % RH), the refractive index for classical 633 nm (red) laser wavelength is 1.000 271 374. Failing to make any correction for refractivity is an immediate error of 2.7 parts in 10^4 or 270 µm/m - after only 4 m of beam propagation the error exceeds 1 mm. Secondly, if there exists a refractive index gradient, caused by a temperature gradient, then a beam propagating through this air will be bent - devices which measure angles of laser beam propagation (such as laser trackers, NPL's optimum system, the CNAM multilateration system) will have to point the beam at an offset angle to hit the target - this leads to a tangential error in the determined position. Fortunately, refractive index can be calculated when the air temperature, pressure and humidity are known. Whilst it is rare to have significant pressure or humidity gradients in a factory volume, temperature gradients are very common - using a typical single point measurement of air temperature does not truly sample along the whole beam length, leading to errors. What is required is a measurement of the air temperature along the measuring beam. Several approaches by different partners have delivered this requirement, with sufficient accuracy to replace the existing single point air sensors. This means that the project has advanced the state of the art in large volume refractive index compensation for optical measuring systems, and satisfied the objective of this part of the project.

Measuring air temperature is a complex problem: contact sensors like Pt100 can have a slow response time, and errors can be induced by a weak thermal link with the air at low flow speeds, or by a stronger than expected radiative environment. Acoustic or spectroscopic thermometry has the potential to solve these is-sues thanks to a direct physical relationship between the speed of sound or light absorption in a gas and its temperature.

VTT Spectroscopic thermometer

The work of VTT presents a highly miniaturized and simplified experimental hardware setup, which could be readily combined with a distance meter into a single instrument. The spectroscopic and length measurement share the commonality of being optical measurements, which greatly benefits system integration. The system realized by VTT differs from previous ones so that separate power modulation is removed from the design and wavelength scan rate is increased. Furthermore, the system is capable of measuring from the same retroreflective targets as distance measuring instruments. In absorption spectroscopy, the signal is often modulated and detected at a single frequency to resolve the absorption signal from noise. No amplitude modulation is applied to the signal in this work, resulting in a noisier signal with larger offsets. Despite this, decent accuracy and precision is achieved by collecting a large amount of data with the compact system. Additionally, the thermometer is calibration-free in the sense that measurement traceability comes from the spectral parameters published in the HITRAN spectroscopic database. The aim is to facilitate reliable measurements in varying environmental conditions, in a manufacturing facility with large temperature gradients, and to realise a system where adjustments or moving the device to a new location does not cause offsets that need to first be measured and removed/calibrated out. The system uses multiple spectral features of atmospheric oxygen, and two DBR-type lasers are used for the scanning. The setup is shown schematically below in Figure 17. The setup is designed with compactness and robustness in mind, with fibre-coupled optical components and miniaturized electronics.

Light from the lasers is split into two arms by a fibre splitter, one of the arms functioning as the reference signal arm and the other as the spectroscopic signal arm. The reference signal is directed to the reference photodiode, while the spectroscopic signal is emitted to free space from one of the ends of the 90/10 fibre splitter. The fibre end is positioned at the focal point of an off-axis parabolic mirror, which collimates the light into a beam of 3 cm in diameter. If the beam is aimed at a retroreflector, it will reflect back and focus back into the fibre splitter. From there, the returning light is finally guided to the signal photodiode. The 90/10 splitter effectively functions as an optical circulator, guiding most of the light returning from air towards the photodiode instead of back to the lasers. The laser diodes incorporate integrated isolators and the small fraction of light returning from air does not disturb their operation.

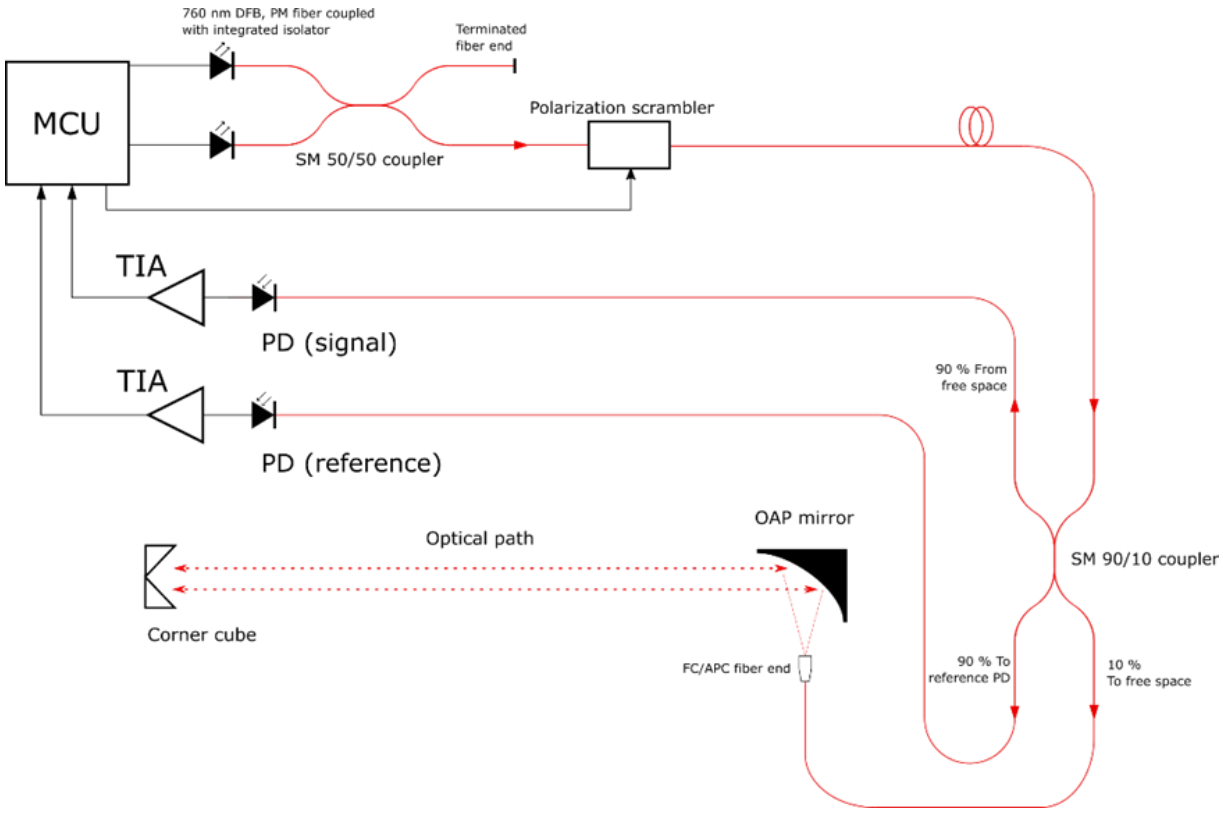

Figure 17 - the final scheme of the VTT spectroscopic thermometer developed in the project. MCU=microcontroller, TIA=transimpedance amplifier, PD=photodetector, OAP = off-axis parabolic mirror

The performance of the thermometer was evaluated by comparing it with an interferometer on a 30 m long interferometric measurement bench at variable laboratory conditions. Both devices were positioned at one end of the bench. The parabolic mirror of the thermometer was placed 5 cm above the interferometric beam, and both beams were targeted at a retroreflector at the other side of the bench. Thus, the beams of interferometer and spectroscopic thermometer increasingly overlapped as they converged to the retroreflector.

To produce an inhomogeneous temperature distribution along the bench, the beams were aligned to propagate through an apparatus consisting of two pipes, set coaxially such that the light beams travel through the inner, metallic pipe. Temperature controlled air is blown inside the outer pipe from the middle, and from there the air continues to flow towards both ends while exchanging heat with the outer surface of the inner pipe. Heat is then exchanged between the inner pipe and the air it encloses, but unlike the layer of air between the outer and inner pipe, the air inside the inner pipe remains highly static. This ensures strong air turbulence will not cause discontinuities in the interferometric measurement. To further avoid turbulence experienced by the beams, the inner pipe extends one metre outside the outer pipe at both ends; the air blowing out of the outer pipe then does not chaotically mix with the air at the entrances of the inner pipe. The length of the pipe system is approximately 10 m, thus constituting one third of the measurement path. The diameters of the pipes are 100 cm and 120 cm p.o. mm for the inner and outer pipe, respectively.

Figure 18 shows results from a 200 minute experiment. The upper graph shows the spectroscopic temperature in orange, and the temperature solved from the interferometer readings are shown in black. The interferometric temperature is calculated from the so-called updated Edlén formula (backwards) for the refractive index of air.

The air turbulence causing spatio-temporally quickly varying refractive index is affected by both the magnitude of the air flow blown inside the pipe system, as well as its temperature with respect to the temperature of the air inside the pipes. Around 130-150 minute mark, strong turbulence caused the microcontroller to discard almost half of the sweep data. This is the reason for the changing “noise level” during the experiment. Also, the laser interferometer and temperature measurement beams do not overlap so there may be small changing differences in the air temperature along the two paths. The temperature difference stayed mostly within 0.2 °C. or 0.3 °C.

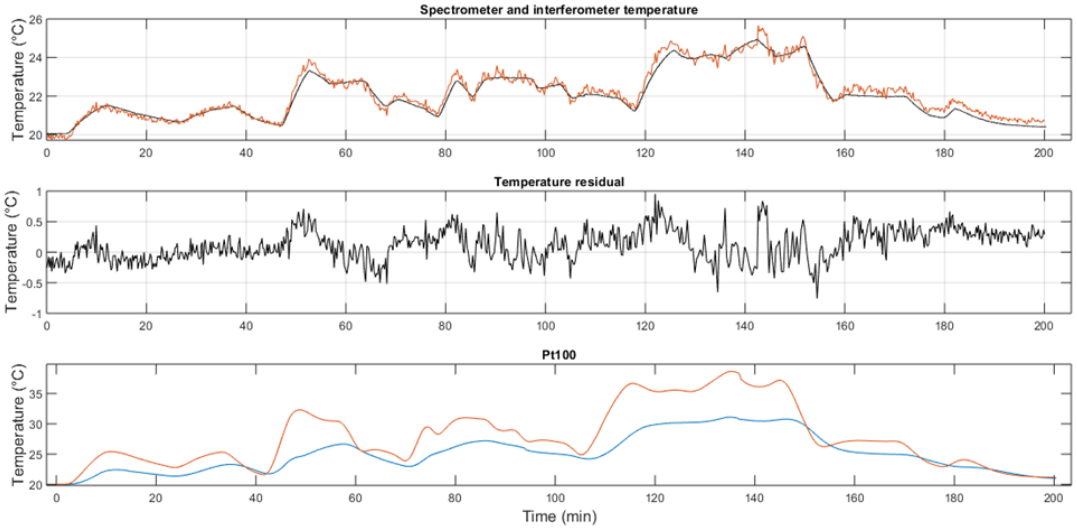

Figure 18 - a test run with variable temperature. The top graph is spectroscopic temperature (red) and interferometric tem-perature (from optical distance change, black), the middle one is the difference, and the bottom graph shows the temperature in the center (red0 and peripherary (bllue) of the heated part of the optical path.

In addition to the experiment presented, the spectroscopic thermometer has been tested also with a wave-length-dependent multiplexer added between the head and the rest of the system. This allows for introducing a distance measurement device running at different optical wavelength (*e.g.* 1.5 µm) to the same measurement head. The results were promising in the sense that the addition of the WDM only added ~100 mK of variation to the spectroscopic temperature result. The effect of the fiber WDM device was also seen as a fine ripple in the obtained spectra.

The temperature accuracy seems to be 0.1 K – 0.2 K in low turbulence conditions, or even better after possible further development of the system.

INRIM continuous-wave acoustic thermometer

INRIM designed and built a thermometer system based around the measurement of the phase delay φ experienced by an acoustic signal, at frequency f, travelling through the air over distance d, compared with the original source signal at the point of generation. The measurement gives directly the speed of sound u at temperature T according to:

$$u\,(T) = d \cdot f/\varphi$$

However localization of the actual point of reference of the source and detector is difficult when using actual hardware (loudspeaker, microphone) and a further complication arises because the phase is cyclical - integer numbers of phase cycles may occur over longer paths and this integer is difficult to determine. The solution to both problems developed by INRIM was to use frequency sweeping. By sweeping the frequency in a given interval, the phase changes continuously proportionally to the distance d. It is easy to see that the relationship between the speed of sound, frequency, phase and distance is:

$$d = u \cdot \delta\varphi/\delta f \tag{18}$$

thus, assuming the linearity of the function $\varphi(f)$, a measurement of the slope $\delta\varphi/\delta f$ allows one to determine the value of d to be used in equation 1. However, this does require *a priori* knowledge of u. Fortunately, this can be obtained by making an estimate of d for a fixed setup of the equipment over a short range (*e.g.* 1 m) - this can be estimated well enough - then, by comparing the system's measurements with those obtained using classical thermometers over the short range, a value can be predicted for u. This allows determination of a more accurate value for d, from which fixed points can be set as fiducials on the equipment corresponding to

the distance *d* and for future measurements the separation between the fiducial locations (*e.g.* the front lip of the speaker, and the microphone mounting collar) can be measured using commercial distance measuring devices such as a Bosh GLM laser distance meter which INRIM calibrated in-house and which offers a 0.1 mm resolution up to 10 m range. The INRIM thermometer is depicted in Figure 19, with both a schematic diagram and a photograph. INRIM chose to use frequencies close to 20 kHz: the relatively high attenuation in the order of 100 dB/100 is partially mitigated by the high directionality that can be obtained in this frequency range and the frequency is mostly inaudible to humans.

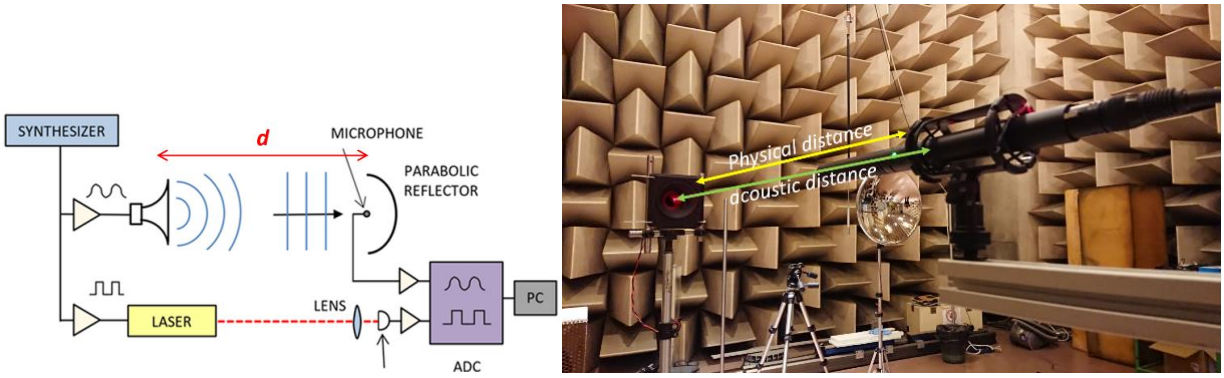

Figure 19 - the INRIM continuous-wave thermometer: left- schema; right -photo.

INRIM tested the thermometer by comparison with Pt100 thermometers placed along the acoustic beam path (plus values of air pressure and humidity obtained using conventional sensors). The first set of tests were performed over an 8.2 m path length. The speed of sound was measured with the acoustic thermometer and compared with results from the recorded environmental (P, T, RH) parameters according to the Cramer equation. Figure 20 shows typical results, when the conditioning system of the laboratory was left switched off. The measurement took about three days and a progressive cooling of the ambient temperature with superposed natural day/night periodic variations were observable. In this case the temperature range was (12 – 18) °C, the RH range was (25 – 47) % and the pressure range was (99.6 - 100.2) kPa. For this measurement run the difference between the measured and predicted speed of sound values was found to be less than 0.06 m/s.

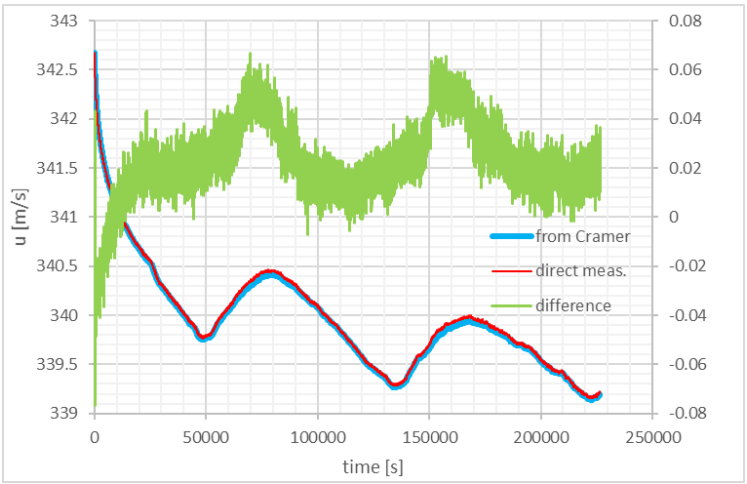

Figure 20 - Comparison between the speed of sound measured by the INRIM therometer and that calculated by Cramer equation over an 8.2 m distance. The blue curve is the speed of sound calculated from the average of the temperature measured by the four thermometers placed along the acoustic path. The red curve is the speed of sound directly measured by the acoustic thermometer. Both curves refer to the left scale in m/s. The green curve is the difference between the two referred to the right scale in m/s.

A second set of tests were performed over the maximum available path length of 11 m and typical results are shown in Figure 21. As with the tests over 8, the best agreement was obtained when the rate of change of temperature was the smallest.

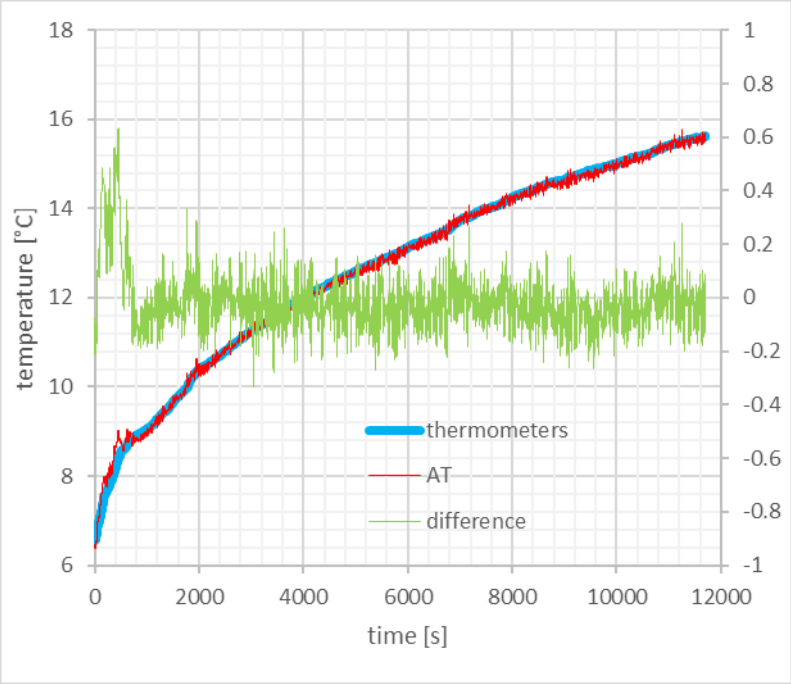

Figure 21 - comparison between the temperature measurement obtained by platinum thermometers and the acoustic thermometer over a 11 m distance. The blue curve is the mean of the temperature measured by the six thermometers placed along the path. The red curve is the temperature estimated from the speed of sound through the Cramer equation. Both curves refer to the left scale in °C. The green curve is the difference between the two referred to the right scale in °C.

The tests show that the acoustic thermometer is delivering air temperature results with an uncertainty of around 0.1 °C.

INRIM performed further tests using two acoustic thermometers (operating a slightly different frequencies) with the thermometers arranged one above the other in order to measure vertical temperature gradients. The tests were performed over a 26 m range and then over a 60 m range. The acoustic thermometers were able to measure a vertical gradient of 0.3 °C/0.5 m and the value obtained agreed with that from conventional Pt100 thermometers to within 0.1 °C.

INRIM has realized a method capable of measuring the speed of sound in air at the scale of tens of meters in a closed environment. The method allows one to estimate the average temperature of air along the acoustic path. The effectiveness of the method has been demonstrated by comparing the acoustic temperature measurement with the same temperature measured by classical calibrated platinum thermometers. Furthermore, the effectiveness of the method for measuring vertical temperature gradients in a large volume by using two acoustic thermometers working in parallel, is demonstrated. The agreement between the two types of thermometry is within 0.1 °C for all the measurements. The accuracy of the comparison is currently limited by the low spatial resolution of the classic thermometers (the distance between the Pt100 probes was about 2 m for each experiment) and to the different time constant of the two methods. These results indicate that the refractive index of air and hence interferometric distance measurements may be performed with a relative accuracy of 10^{-7}. This can be used to deliver better accuracy for optical distance measuring systems *e.g.* laser trackers than can be obtained using the usual single point sensor supplied with such instruments.

CNAM pulsed acoustic thermometer

A third approach to measuring the temperature of the air along a measurement path was followed by CNAM, who developed an acoustic thermometer, but unlike INRIM, CNAM used a pulsed system. Again, the operational principle is based on the time of flight and the effect of temperature on the speed of sound.

The speed of sound depends on the air temperature, and to a lesser extent on the atmospheric pressure and the humidity and CO_2 contents. The Cramer equations describe the speed of sound directly as a function of these environmental parameters.

$$v_0(\theta, p, x_w, x_c) = a_0 + a_1\theta + a_2\theta^2 + (a_3 + a_4\theta + a_5\theta^2)x_w + (a_6 + a_7\theta + a_8\theta^2)p + (a_9 + a_{10}\theta + a_{11}\theta^2)x_c + a_{12}x_w^2 + a_{13}p^2 + a_{14}x_c^2 + a_{15}x_w p x_c$$

Here, θ is the air temperature expressed in degree Celsius, p the atmospheric pressure, x_w the water vapor mole fraction, and x_c the CO_2 content. The coefficients a_0 to a_{15} are provided by Cramer - they were determined empirically by Cramer for the temperatures from 0 °C to 30 °C, static pressures from 750 hPa to 1020 hPa, up to 0.06 water mole fraction and up to 1 % of CO_2 concentration. More recent work has revealed that these equations have an uncertainty of 545 ppm (5.45×10^{-4}).

In practice, in order to determine the speed of sound in the air, the CNAM acoustic thermometer measures the time of flight t_{TOF} of acoustic waves travelling in the air over a known distance d.

$$v_m = \frac{d}{t_{TOF}}$$

By measuring the speed of sound, v_m, using conventional cheap sensors for air pressure and humidity content and then back-calculating using the parametric equation for $v_0(\theta, p, x_w, x_c)$, one obtains the air temperature θ. In order to cancel uni-directional airflow effects on the speed of sound, the CNAM system used bi-directional measurement in which one beam is positively affected by the airflow, and the other beam is negatively affected, cancelling out. A schematic of the CNAM system is shown in Figure 22.

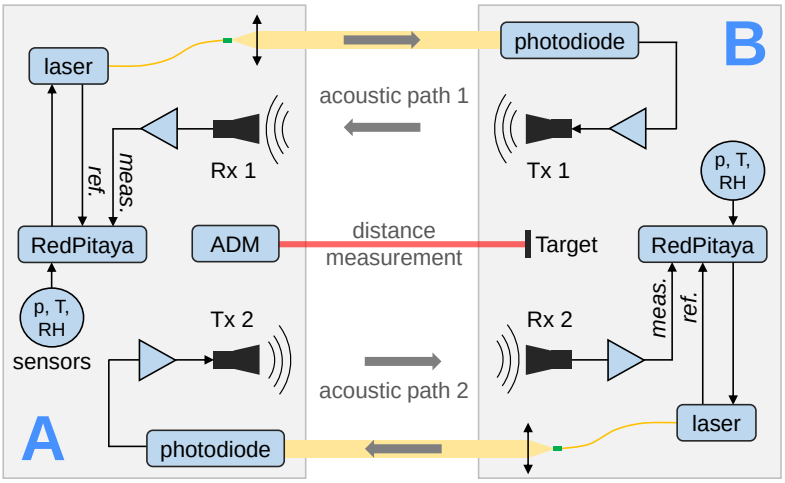

Figure 22 - schematic of the CNAM pulsed air path thermometer. ADM - absolute distance meter.

The CNAM system uses two pairs of ultrasonic transducers operating a transmitter/receiver pairs, an absolute distance meter (a Leica disto 210, for measurement of *d*) and commercial sensors for air pressure, single point temperature, and relative humidity. An image of the 'A' half of the CNAM system (as depicted in Figure 22) is shown in Figure 23.

User comfort requires inaudible acoustic frequencies. Thus, ultrasonic frequencies around 40 kHz have been selected. At such frequencies, the used transducers are compact, widely available on the market, and offer a good directivity. However, sound attenuation in air is about 1.3 dB per meter: to increase the power transmitted to the receivers, horn antennas have been used for the acoustic emission as shown in Figure 23. The adopted signal is an acoustic pulse of 500 µs duration with a repetition rate of 119.2 Hz and a linear frequency modulation (chirp) from 38 kHz to 42 kHz. In order to record the reference signal and the measurement one on the same capture, the *RedPitaya* data analysis boards generate an acoustic pulse every 8.389 ms, *i.e.* with a 119.2 Hz repetition rate. For distances longer than 2.8 m, more than one pulse cycle will have elapsed since transmission, so an integer order has to first be estimated using the data from the commercial sensors and the

distance from the ADM. Due to using low-cost components the low signal to noise ratio requires techniques including cross-correlation and cross-spectrum processing to be used. Lastly, the system switches between the two paths every 2.5 seconds to cancel out the effects of airflows or wind.

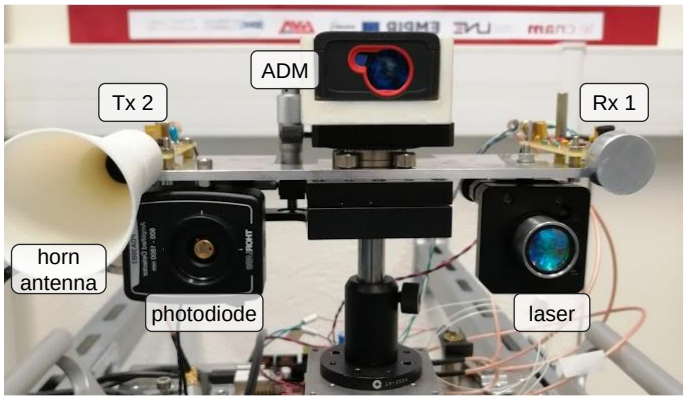

Figure 23 - part A of the CNAM sensor, as labelled in the preceding figure.

A test of the system over an 8.471 m room at 23 °C gave residuals of only 1.5 µs when using a cross-correlation technique and 2.5 µs when using a cross-spectrum technique. These values can be regarded as the repeatability of the CNAM acoustic thermometer, i.e. the standard deviations on measurements made over a short period of time, at a fixed temperature, for the same distance, with the same system, under the same operating conditions. The intercorrelation technique did show occasional rogue values but these are not present in the cross-spectrum analysis. The intercorrelation technique is used to obtain the best data and the other technique is used to baseline the intercorrelation technique to allow removal of rogue points. Internal propagation delays in the electronics and optics were calibrated out by measurements performed over ranges up to 10.6 m - they appear as a fixed offset on all time of flight measurements and the value is easily obtained.

After calibration the CNAM thermometer system was tested over the same set of ranges up to 10.6 m used for the estimation of the internal delay offset. The results, shown in Table 2Table 2, indicate that the thermometer is achieving a standard uncertainty of between 0.09 °C and 0.13 °C, which is comparable with classical Pt100 probes used on *e.g.* laser trackers which have a standard uncertainty of 0.1 °C; however the CNAM system measures the true along-the-path temperature and the Pt100 probe only measures a single temperature of wherever it is located.

Table 2 - test results for the CNAM acoustic thermometer.

Distance (m)		3.318	5.012	7.368	8.984	10.718
Uncertainty on the measured temperature (°C)		0.13	0.12	0.12	0.09	0.09
Tested temperature range (°C)		5.0	3.5	4.0	4.5	4.0
residu-als	Average value (°C)	-0.10	0.06	0.05	0.07	0.23
	Peak to valley variation (°C)	0.20	0.25	0.40	0.30	0.20
	Standard deviation (°C)	0.2	0.1	0.1	0.1	0.1

In summary, the three systems described above perform measurement along an optical beam to a target/reflector, mimicking the dimensional measurement approach of many LVM devices. As such, they sample the true along-the-beam refractive index which is needed to compensate deliver 0.1 °C to 0.2 °C along-the-beam accuracy and the INRIM system has demonstrated 0.1 °C vertical gradient measurement accuracy. With the refractive index temperature sensitivity $\partial n/\partial T$ being 9.2 × 10-7 $°C^{-1}$, these systems deliver the target accuracy of ~10^{-7} which was the basis for the technical objective for this part of the work.

4.4 Development of models to simulate self-organising production and assembly based on digital information from process-integrated measurement systems and application of these methods to other project outputs to produce an industrial scenario demonstrator.

Metrology-assisted manufacturing and assembly have been identified as promising approaches to address issues of smaller lot sizes, elevated tolerance requirements and provide more intelligent automation. Especially in assembly, the underlying idea is to replace the spatiotemporal synchronization, which is typically provided by fixed layouts and monuments, by metrological reference information, predominantly Large-Scale Coordinate Metrology. As such, a ubiquitously available reference coordinate system becomes an infrastructural component. However, there are three main challenges that emanate:

1. The required metrological capabilities greatly vary, *e.g.* in terms of achievable uncertainty, covered volume, concurrency of measured targets, dynamic usability, traceability. At the same time, the overall system is subjected to economical constraints such that using high-end metrology systems alone is expected to be prohibitive. This leads to individual systems (*e.g.* indoor GPS) reaching their technological or economic limits when scaling metrology-assisted systems beyond individual setups towards an entire shop floor.
2. Metrology-assisted applications are often designed as individual, closed system, addressing one specific problem and performing the integration specific to the application and metrology system under question. This impedes true flexibility and reconfigurability.
3. Production systems are becoming more and more interconnected in general with the shift towards Cyber-Physical Production Systems (CPPS). Hence there is a need for integration information of metrology systems into the data ecosystem of CPPS. Therefore, metrology systems and software stacks need to become interoperable.

The state-of-the art software system for the distributed, heterogeneous Large-Scale Metrology systems is constituted by applications like *SpatialAnalyzer, PolyWorks, Metrology, Verisurf* or *BuildIT*. While they are very well suited to implement individual applications and inspection tasks, they are not a priori designed to provide a permanent reference coordinate systems for multiple, potentially unknown applications. Moreover, the integration metrology systems into these software products still depends on individual programming efforts based on the proprietary interfaces of the respective systems. Lastly, the integration into modern data ecosystems and industrial IoT protocols such as OPA UA, MQTT, REST etc. remains unsolved by these systems but is crucial to ensure a strong position of metrology systems in the future.

The challenges mentioned above have been addressed in the LaVA project by introducing the Coordinates as a Service (CaaS) paradigm and developing the following components:

- A model-based, protocol-agnostic, service-oriented interface to Large-Scale Metrology systems allowing for unified interfacing and decoupling the use of a specific system from its software integration.
- A metrological capability model to map requirements of production processes to available metrology systems capable of providing the required position information.
- A service-oriented architecture incorporating all required components to provide position information and hence Coordinates as a service.

These components will be described in greater detail over the following paragraphs.

Model-based, protocol-agnostic interface

The unified device interface was designed using the Sensor Interfacing Language SOIL (DOI:10.1007/978-3-662-62138-7_45), a domain-specific language that was developed by RWTH Aachen Cluster of Excellence *Internet of Production*. The chosen approach decouples the unified modeling of different Large-Scale Metrology systems, the general information model for sensor systems, and the communication using standardized protocols. To further reduce complexity and provide concise representations, a division of resources into Objects (OBJ), Functions (FUN), Variables (VAR) and Parameters (PAR) only offering specific subsets is proposed: *Objects* provide an object-oriented data view and in combination with structured identifiers are the only resources allowed to possess subordinate child items. *Variables* encapsulate access to data with physical origin, *e.g.* measurements, which are naturally read-only. *Parameters* separately encode read and potential write access to primitive data fields. *Functions* are resources that are callable with a set of argument and return values, leading to a function invocation on the resource.

The overall organization of SOIL is hierarchical, using locally unique identifiers (*uuid*) which can be concatenated to a fully qualified identifier, which *e.g.* serves as a URL. Only Objects are allowed to have child items. Each resource types comes with a defined set of metadata to ensure high data quality, especially for long-term objectives.

For the unified modelling of Large-Sale Metrology systems, a functional view from an application's perspective was adopted over a physical view exactly representing the embodiment of the system. Hence, a Large-Scale Metrology system is modeled as:

- A set of **base stations**, which are fixed and have an enabling role. In case of a centralized system, there is exactly one base station. Examples are a laser tracker head, indoor GPS transmitters, OPTIMUM Heads or distributed cameras. A fixed-type kinematic, as *e.g.* for CMMs, is also interpreted as base station.
- A set of **mobile entities**, which corresponds to the targets whose positions are measured. In the information model, the measurement of the current position is always retrieved through the corresponding mobile entity, even if it is effectively measured at the base or through multilateration or multiangulation. Examples are SMRs, $n = 2$ spheres, indoor GPS PCEs, or photogrammetric targets.

This approach organizes the entire information model under four elements:

- **Root** The root object is the entry point for the Large-Scale Metrology as general device, accommodating elements which are rather general (*e.g.* Startup and Shutdown).
- **LSM** The Large-Sale Metrology (LSM) objects represents the model briefly described above. It can be integrated into more complex models and therefore is a node on its own.
- **Entity** For each mobile entity, an own object containing the relevant functions, parameters and variables is present. Each entity has an *uuid* to address it.
- **Base** For each base station, an own object containing the relevant functions, parameters and variables is present. Each base has an *uuid* to address it.

SOIL is protocol-agnostic by definition, *i.e.* it may be mapped to HTTP/REST, MQTT, OPC UA, grpc.io and many more. Within LaVA, the mapping to HTTP/REST and MQTT using JSON for serialization has been used and successfully evaluated. During the development phase, it was applied to an API Radian 3™ laser tracker, a Leica AT960™ laser tracker, a Nikon/7DK indoor GPS system, a Pozyx UWB system and a Machine Tool. During demonstration (*cf.* 4.6), additional integrations were added. A full representation of the Large-Scale Metrology Interface Model is publicly available as OpenAPI specification at https://git-ce.rwth-aachen.de/wzl-mq-public/soil/schemas/large-scale-metrology/-/blob/main/public/openapi.yml. C++ and Python libraries to apply SOIL to other metrology systems have been made available open source under an MIT License at https://git-ce.rwth-aachen.de/wzl-mq-public/soil. The device interface has been reviewed by project partners including SAAB.

Metrological capability model

The capability model was derived based on a literature review and expert knowledge within WZL | RWTH Aachen incorporating the works of CAI *et al.* (2010), MULEANER *et al.* (2010), MAROPOULOS *et al.* (2008), FRANCHESCHINI *et al.* (2014) and NICKSCH *et al.* (2020). The synthesis is, like the model-based interface described above, mobile entity centric and is summarized in the table below:

Name	Symbol	Description
Position Coverage	$\mathcal{B}(\hat{\boldsymbol{p}})$	Boolean response function whether a mobile entity is able to measure at $\hat{\boldsymbol{p}}$.
Angular Acceptance	$\mathcal{Q}(\hat{\boldsymbol{p}}, \hat{\boldsymbol{n}})$	Boolean response function whether at $\hat{\boldsymbol{p}}$ the target is able to measure at an orientation expressed as normal vector $\hat{\boldsymbol{n}}$, e.g. for scenarios with rotating end effectors.
Covariance Prediction	$\hat{\boldsymbol{V}}(\hat{\boldsymbol{p}}, \hat{\boldsymbol{q}})$	Prediction of the covariance matrix at $\hat{\boldsymbol{p}}$, e.g. model-based. The anticipated velocity $\hat{\boldsymbol{q}}$ is designated for uncertainty models reproducing dynamic characteristics.

Transformation Covariance	$\hat{\mathbf{S}}(\hat{\boldsymbol{p}})$	Estimated covariance contribution due to the transformation to global coordinates at $\hat{\boldsymbol{p}}$.
Measurement Time	$t_{measure}$	Time required per measurement, e.g. for estimating uncertainty induced by motion.
Dead Time	t_{dead}	Estimated time between physical measurement and its delivery via the interface.
Sample Frequency	f_{sample}	Maximum possible frequency for measurements, including dead times, e.g. for designing control loops.
Maximum Target Velocity	v_{max}	Maximum velocity the target is allowed to move while measuring.
Environmental Limits	$\{T_{min}, T_{max}\}\{p_{min}, p_{max}\}$ $\{H_{min}, H_{max}\}$	Limits for temperature (T), pressure (p) and humidity (H) allowed during correct operation.
Orientation Measurements	$\mathcal{O}$	Boolean indication whether the orientation of the mobile entity is captured.
Target Type	$\mathcal{F}$	Type of the mobile entity as one of {reflector, marker, natural feature, probe, complex}.
Exclusiveness	$\mathcal{R}$	Boolean indication whether using the target disables other targets of the system (e.g. for a laser tracker).
Traceability	$\mathcal{T}$	Boolean flag whether measurements from this instrument are traceable
Mobility	$\mathcal{K}$	Boolean indication whether the entity can be attached to a moving unit or is moved by a fixed kinematic (e.g. CMM)
Scanning	$\mathcal{Z}$	Boolean indication whether the entity is representative for a point cloud measurement (e.g. laser radar)
Cost Factor	$\frac{\partial \mathcal{C}}{\partial t}$	Additional variable cost per time for using the target/instrument.

In contrast to the state of the literature, the approach assumes that position coverage, angular acceptance and covariance prediction are based on actual models predicting the behaviour of the Large-Scale metrology system in application. Both the metrology systems and the application use the set of parameters described in the table above to model offerings and requirements. It is expected that $\hat{\boldsymbol{p}}, \hat{\boldsymbol{q}}$ and $\hat{\boldsymbol{n}}$ are derived from planned trajectories or reference locations.

In addition, a JSON representation of the capability model has been elaborated such that it can be unambiguously used in queries by both process modeling software and microservices managing the different Large-Scale Metrology instruments as resources of CaaS. For demonstration purposes, such a microservice simultaneously acting as scheduler has been implemented using Python and the Django Rest Framework (https://www.django-rest-framework.org/)

Service-oriented Architecture

To cope with the requirements of modern manufacturing IT and leverage the potential benefits of Cloud and Edge Computing for metrology assisted applications, a decomposition of the overall CaaS system into microservices has been proposed and is outlined in the Table below. Retrospectively, this certainly is only possible implementation and usage of modern IoT ecosystems and should be regarded as example how the domain of (Large-Scale Coordinate) metrology could integrate with these. The repartition of microservices among different layers of an IoT system, which corresponds to the reference implementation, is shown in Figure 24.

Symbol	Name	Description
$\mathbb{I}$	Instrument	The functionality respectively operation of the individual Large-Scale Metrology instruments is encapsulated in microservices as defined above.
$\mathbb{C}$	Consumer	Any application utilizing the CaaS system is regarded as a microservice on its own, which either directly interacts with human users and agents to physical actors or represent services themselves, e.g. persistent data storage and analysis or geometric characteristic evaluation.
$\mathbb{M}$	Modeling	The appropriate estimation of the expected covariance and other capabilities discussed above requires implemented, queryable models of the instruments. As the mathematical formulation may be opaque to the relying parties, this requirement effectively instantiates a microservice. This component is a prominent example for a situation where the microservice may be provided on an external platform, e.g. hosted online by the instrument's manufacturer or a national metrology institute.
$\mathbb{U}$	User	Consistent authentication and authorization among multiple microservices requires a shared user directory, which is regarded as a service by itself. It is expected that in many cases a centralized accounting system will be available independently of CaaS.

$\mathbb{E}$	Entity	This microservice maintains records of the instruments' entities available to the CaaS system including their capabilities and the coordinate transformation parameters among each other. Therefor it relies on the instrument modelling microservice(s) $\mathbb{M}$.
$\mathbb{A}$	Allocation	The formal resource allocation business consists of ensuring that no interference between multiple consumers using the CaaS with individual instruments as resources occur, mainly by keeping track of access requests over time. In consequence, the allocation microservice must provide an interface both to consumers demanding an allocation as well as instrument microservices checking the access right on a consumer. In the case of user-grained authorization scenarios, this microservice may interact with the user service.
$\mathbb{P}$	Planning	The actual choice of a mobile entity and/or is a multi-constraint optimization problem. Its encapsulation as a microservice allows to defer this task to a superordinate resource management system, while an implementation within the CaaS system is still possible and necessary to deliver position information as a service result to arbitrary consumers.
$\mathbb{X}$	External	To maintain compatibility, any custom extension or modification to the CaaS system is encouraged to be implemented as a separate microservice rather than substituting one of the base services. Moreover, this software software design facilitates the development of third-party modules. An example could be an application analyzing the expected visibility impacts on optical measurement instruments based on current CAD-Models of the shop floor.

Table 3 - decomposition of the overall CaaS system into microservices.

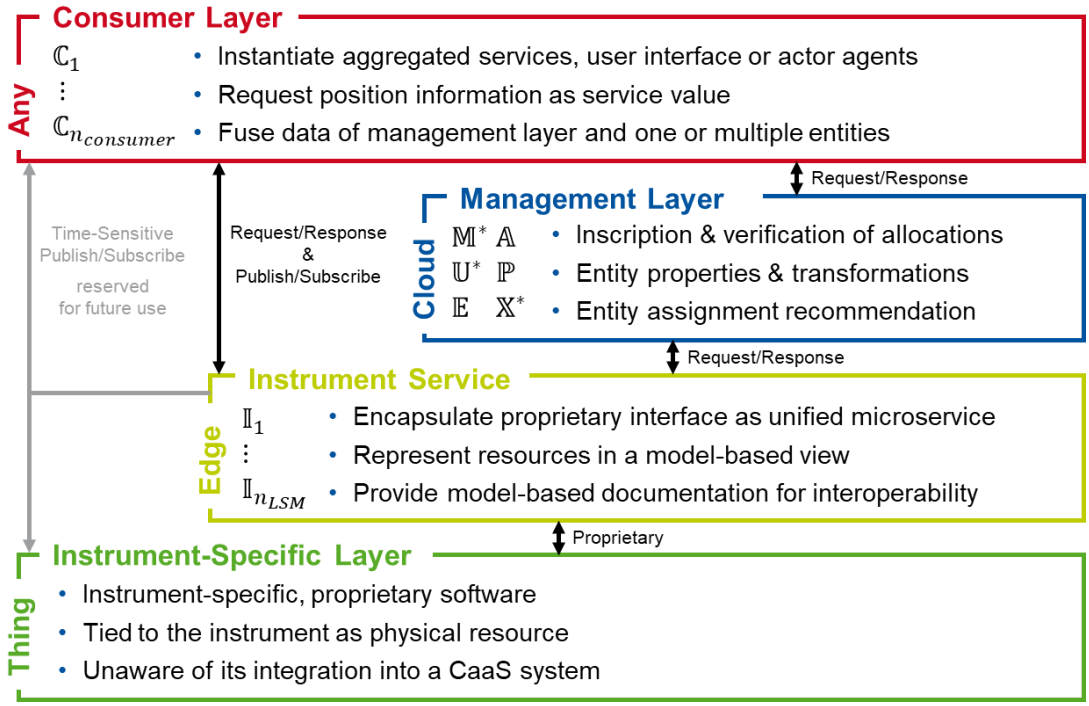

Figure 24 - repartition of microservices among Thing, Edge, Cloud and Service Consumer Layer.

Prior to the demonstrator activities, a full CaaS reference implementation has been realized at WZL | RWTH Aachen's laboratory shopfloor using an in-house data centre as backbone. Among the applications implemented as CaaS consumers, a Machine Tool Calibration routine, tracking of collaborating robots and a bridge to the Robot Operating System ROS have been realized.

Overall, the completion of the research objectives described in this section can be evaluated as successful, satisfying the fourth objective of the project concerning process-integrated measurement systems modelling. Among the impact created by this objective and its adherent work packages, a PhD Thesis has been completed at WZL | RWTH Aachen which is openly accessible and provides more detailed insights (https://doi.org/10.18154/RWTH-2021-10238). At the time of writing this report, the developed architecture and model-based interfacing approach are both gaining interest on their own, hence also partial artifacts of CaaS can be considered as valuable output of the project.

4.5 Production of equipment and validated methods for evaluating the performance and compensating for the errors of large machine tools (> 50 m³); the cost and operability being adequate to leave the equipment on board or on the shop floor.

Modern large machine tools often feature multiple axes of motion, both rotary (spindles) and translation (linear slideways). In theory, these axes are mechanically aligned to be mutually orthonormal. In practice, small angular errors and positioning offsets occur due to manufacturing and assembly tolerances. These errors should be measured to sufficient accuracy and compensated in the numerical control. Traditional techniques using mechanical probes, straight edges, autocollimators, levels, *etc*. have been in use for many years. More recently, laser trackers or tracers have been also used. Deconvolution of the measured 3D grid into fundamental error components (straightness, yaw, pitch, roll, *etc*.) leads to a parametric model of the geometrical errors, which can be stored in the machine controller and used to derive correction vectors.

A recognised geometry error model is described in the literature. It is called *rigid body model* as it is based on the assumption that the parasitic movements of the three carriages are independent of each other as they were perfectly rigid. Such model is

$$\boldsymbol{e} = \boldsymbol{t}_x + \boldsymbol{t}_y + \boldsymbol{t}_z + \boldsymbol{r}_x \times \boldsymbol{h}_x + \boldsymbol{r}_y \times \boldsymbol{h}_y + \boldsymbol{r}_z \times \boldsymbol{h}_z$$

where the 18 errors composing the vectors $\boldsymbol{t}$'s and $\boldsymbol{r}$'s are functions of a coordinate each, and the effective Abbe arms $\boldsymbol{h}$'s transform the rotations into position errors.

There are two problems with measuring the geometry errors: the effort level, equipment expense and expertise required for the measurements precludes their repeated use; and most machine tools receive infrequent error mapping or even none at all, apart from simplistic linear compensations along the three axes. This is unfortunate and ironic, because geometry error compensation routines are available in most Computer Numerical Controllers (CNCs). The impediment is the derivation of the actual error parameters – the so called *error map*.

The aim of the INRIM's and FIDIA's work in LaVA was to develop a lower cost technique and hardware, which could be left *in situ*. INRIM gained experience in the previous EMRP LUMNAR project. A device named InPlanT was developed to measure coordinates in space contactless by three independent devices, each measuring a position component of a target in space. This was based on a tracking mechanism of the target made of a linear stage carrying a rotary table. The original idea in LaVA was to use the machine tool axes as the linear stages and to attach a rotary table to the ram.

The development of the subsequent prototypes indicated that a rotary table was neither necessary nor desired and that a great simplification of the instrument scheme and procedure was possible. The instrument measures the lateral displacement of a target while the machine carriage moves away along the line of sight of the instrument. This is effectively a straightness measurement. This gave new light to the instrument as well as to how to derive the geometry errors.

The concept of the InPlanT device was based on a collimated laser beam impinging on a spherical retroreflecting target. The retroreflected beam had been studied thoroughly in the previous LUMINAR project. It exhibits a central symmetry in the form of a series of concentric rings with a central spot. The symmetry centre occurs on the line parallel to the impinging beam through the target centre. Detecting the symmetry centre effectively detects the lateral position of the target. In the LUMINAR project the centre detection was carried out by a camera and vision algorithms. This proved effective but not sufficiently accurate particularly when the target was more than a couple of metres away from the device. To improve the accuracy, the prototypes developed in LaVA introduced a mechanical modulation.

The first concept design was based on a rotating disc with slits for beam transmission and timing signals. Two signals were observed: of a digital switch, which gave the time base, and of the retroreflected beam, as integrated by a collimating lens. The slits for the retroreflected beam and for the digital switch were in phase on the disc, so the target is deemed as centred on the line of sight when the two signal peak in phase. Any phase separation of the two peaks measured the displacement of the target relative to the zero. The phase measurement was carried out by cross-correlating the retroreflected signal with a synthetic signal centred to the digital switch. A sensitivity of 0.12 µs/µm or 15 µrad/µm was detected at 1.45 m distance of the target, with a noise of 0.9 µs resulting in a resolution of about 8 µm.

Two limitations were met: the overall size and the achievable resolution. The rotation of the slit when chopping the beam was undesired, ideally it should have been a pure translation. To minimise the rotational effect, a large disc diameter was necessary (∅ 200 mm). The instrument was blind over most of the rotation period, it detected a signal only when the slit chopped the beam, which is a tiny time fraction. This required either very fast signal detection or a low rotation speed, with an unavoidable trade-off between resolution and throughput.

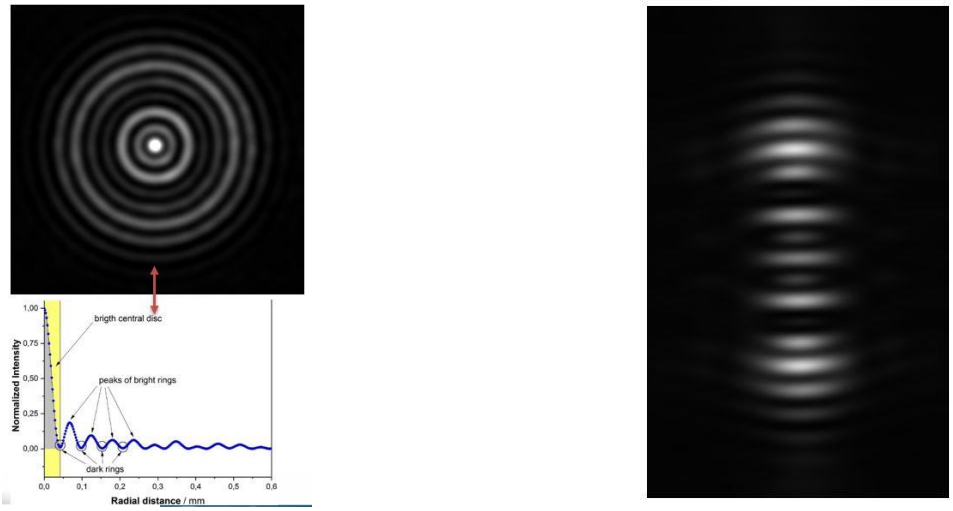

Figure 25 - typical patterns returning from a n = 2 sphere, before (left) and after (right) crossing a 2 mm wide rectangular slit.

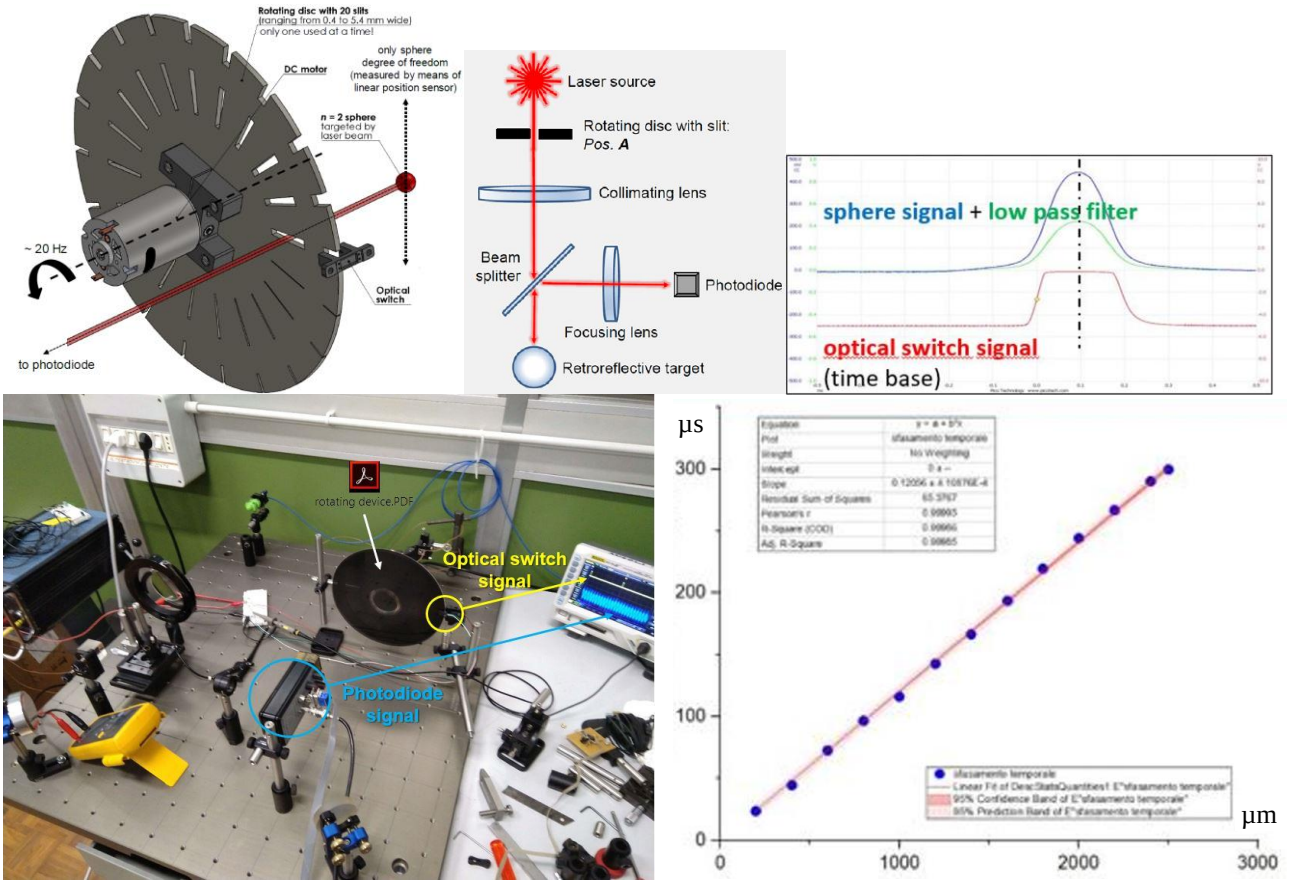

Figure 26 - first conceptual design of InPlanT: (a) rotating disc; it exhibits many slits to investigate the best width, but one only was selected and used. (b) Rotating disc optical scheme. (c) Signals from the retroreflected beam and the digital switch. (d) First experimental set up. (e) Sensitivity study: target later displacement vs. phase shift of the returned peak.

The second concept design replaced the rotation with an oscillation of the slit. Several oscillating drive concepts were investigated and finally the solution of a crank and connecting rod was chosen. The oscillating drive was realised mostly with a 3D printer, with a steel linear stage to drive the motion. The signals changed with this configuration. At each cycle, two retroreflected peaks were detected instead of one, as the slit chopped the beam twice in opposite directions (right and left peaks). When the target was centred, the right and left peaks were equidistant to each other. As soon as the targets got displaced, the right peaks moved to the right,

and the left peaks to the left. This asymmetry conveyed the phase information. The identification of right and left peaks was made on the observation of the digital switch. Again, cross-correlation was used to detect the peak positions.

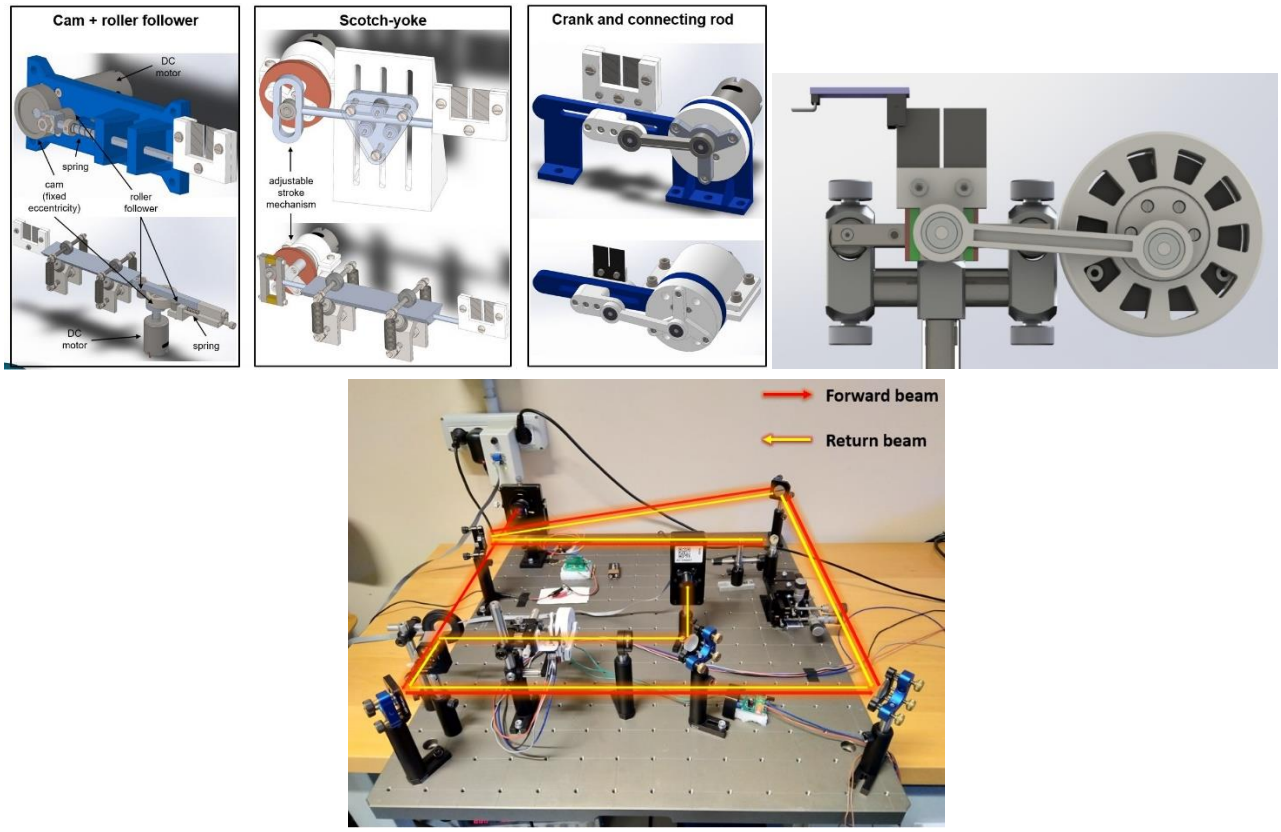

Figure 27 – second conceptual designs of InPlanT: (a) Different oscillating drive concepts investigated. (b) The crack and connecting rod solution adopted. (c) The experimental set up. The beam was bended repeatedly on a breadboard to simulate large target distances.

The main limitation of this prototype was a significant jitter in the oscillation period. Even if in principle each oscillation period was a self-contained measuring cycle with the jitter effect mostly rejected by normalisation, the jitter was still limiting the overall performance.

A third prototype was then designed and manufactured. It was based on the same working principle of the second but with an engineered set up. This prototype miniaturised the design to a size of (300 × 300 × 175) mm³.

Figure 28 - InPlanT engineered prototype (a) Crank and connecting rod drive. (b) CAD design. (b) Physical realisation.

The most relevant metrological characteristic of the instrument was identified in its straightness error. This is the indication of the instrument when the target moves along a perfectly straight trajectory aligned to the line

of sight. To characterize this metrologically, the movable table of the high-precision CMM (Coordinate Measuring Machine) available at INRIM was used as a reference mover. This limited the investigation to the 1.2 m stroke. Preliminary investigation confirmed that the parasitic movement of the table was negligible for this experiment. The target was attached to the carriage and the device to the CMM base. After alignment, the indication of the instrument was observed with the target moved by the CMM table. To transform the phase measurement to a lateral displacement measurement, a preliminary calibration was carried out. The target was attached to a lateral slider and a precision LVDT measured its displacement. The indication of the instrument was recorded at five positions of the target laterally spaced 0.5 mm to each other to cover a range of ±1 mm. A least-square response line was derived. This was repeated at 9 distances to the target with increments of 150 mm to cover the available range (0 – 1.2) m. This calibration values were then used by interpolation. At any target distance, the immediately longer and shortened distance among those explored in the calibration were identified. The responses of the two related least-squares lines were evaluated at the instrument reading value and the two resulting values were interpolated according to the actual target distance. A full independent scan of the stroke was carried out with 16 points in steps of 80 mm. The result was a straightness error of ±6.5 µm, which is mostly in line with the project objective, even if tested on a limited distance only.

The calibration results (see Figure 29 (c)) showed that the response was not exactly the same at all target distances, as the slopes vary. This was because the beam retroreflected by the target sphere is slightly divergent and there is no single direction, rather a range. A position existed where all calibration curves coincided – likely the natural origin of the instruments – and where the LVDT happened to indicate 500 µm. The measurements illustrated in Figure 29 (d) were taken with the target in the lateral position corresponding to the LVDT null indication. There was no time to repeat the experiment; a significant improvement of the result is expected when properly using the instrument close to its natural zero.

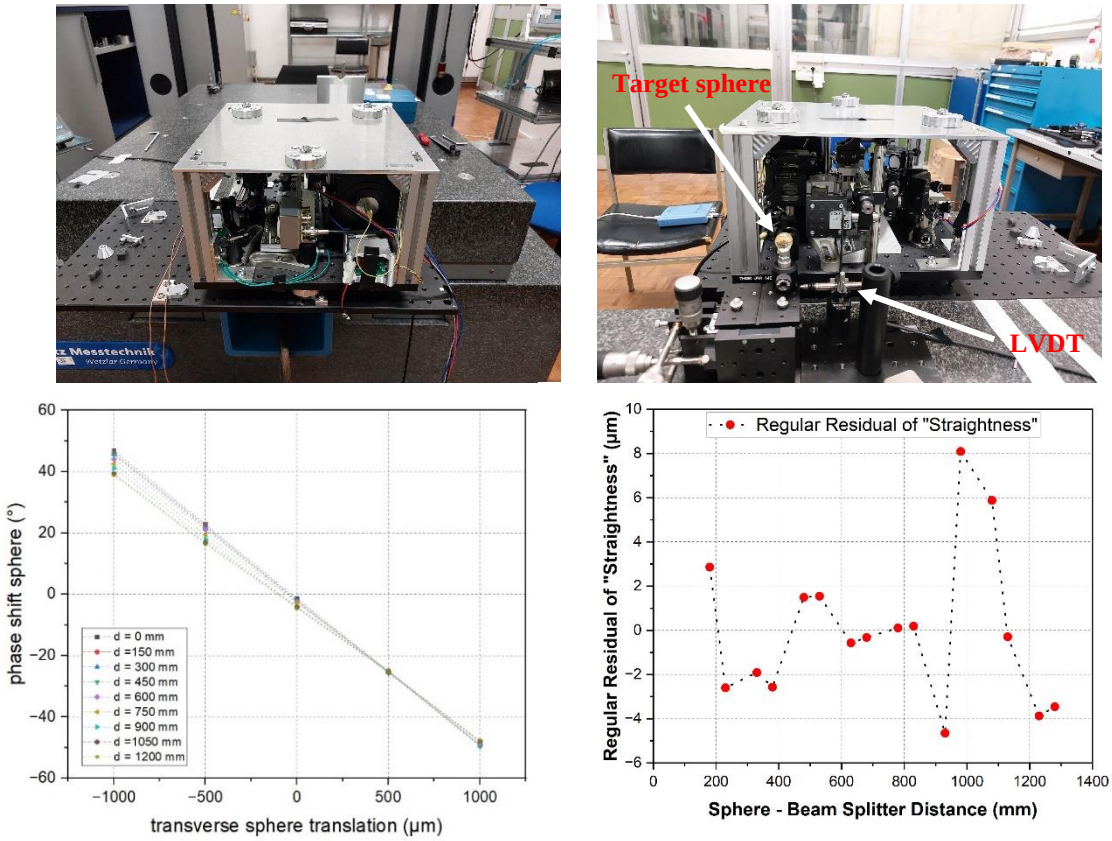

Figure 29 – characterisation of the instrumental straightness error. (a) Device attached to the CMM basement. (b) A front detail of the target in its closest position and of the LVDT used for the calibration. (c) Results of the calibration. (d) Straightness error.

The intended use of the device was to derive the geometry errors, so called *error map*. Aside the rigid body model, another model was needed, referred to as *procedural model*, to reflect and capture the experimental measurements and set up. This resulted to be

$$\boldsymbol{n}_{0j}^{\mathrm{T}}\boldsymbol{e}_{ij} = \hat{\ell}_{ij}$$

where $\boldsymbol{n}_{0j}^{\mathrm{T}}$ is the approximation of the sensitivity direction of the instrument for the j-th line, $\boldsymbol{e}_{ij}$ is the geometry error expressed by the rigid body model at the i-th point of the j-th line, and

$$\hat{\ell}_{ij} = -\boldsymbol{n}_{0j}^{\mathrm{T}}\boldsymbol{s}_{ij} + \ell_{ij} - \beta_j\xi_{ij} - h_j$$

is the combination of the scale readings $\boldsymbol{s}_{ij}$ and the device reading ℓ_{ij} at the i-th point of the j-th line after subtraction of the least-squares line $\beta_j\xi_{ij} - h_j$ relative to the j-th line. ξ_{ij} is the abscissa along the line with an arbitrary origin. Note that, after subtraction of the least-squares line, the above equation introduces no unknowns in addition to those of the rigid body model.

This model was intended to be part of a broader software suite. This is a simulation tool to accelerate the development phase and the definition of the detailed procedure with no need of repeated experimental campaign on real machines. Unfortunately, the time limitation of the project impeded the actual implementation of the above architecture, and some portions only were developed.

FIDIA, a machine tool manufacturer with a facility close to INRIM, cooperated with INRIM in two aspects: helping define the data interchange format for sending data from InPlanT to the machine tool controller of a FIDIA machine tool; and offering to host a test/demonstration of the InPlanT system on one of their machine tools. FIDIA worked with INRIM to define the software architecture for the InPlanT system. A format was required for the exchange of data between the INRIM and FIDIA systems. A parser tool was developed for performing the error map translation. The software architecture for the Procedure Executor (used for machine control) was defined and developed by FIDIA in collaboration with INRIM. This tool runs on the FIDIA CNC front end and allows the automatic cycling through the proposed measurement points and moves the machine axes to the required positions. FIDIA identified the machines on which to validate the method and designed a mounting system for the InPlanT engineering prototype based on their existing interface clamp for laser cutting tools.

Unfortunately, at the half-way part of the project COVID-19 restrictions were enforced: laboratories at INRIM were closed and orders for machine tools dried up and FIDIA paused operations. This meant that in the later stages of the project, when INRIM was preparing to test their work at FIDIA, not many machine tools had been produced and the selection available for use was therefore restricted. Additionally, INRIM ran out of time in the project (due to delays fundamentally caused by the COVID-19 pandemic) and was unable to compare the results of testing on a machine tool at FIDIA with a known error map, as neither the reference error map nor the software to convert from measurement data to an error map were completed in time.

In conclusion, a device for the measurement of the straightness was designed, developed and tested. This followed a sequence of prototypes. The working principle of such device is the mechanical modulation of the response to the retroreflected beam, which allows a fine detection of the beam centre position.

The device was characterised up to 1.2 m of distance. A maximum error of indication of ±6.5 µm was detected, but it is believed that a more careful repetition of the validation experiment would have led to significantly better results. In all cases, the result is compatible with the project target, even if over a shorter distance than originally planned.

The device prototype is currently (300 × 300 × 175) mm³ in size but can be further miniaturised in a next prototype. This is already compatible with machine tools of the dimensions targeted in the project.

The data reduction requires an error model and software. The former was developed but the latter was investigated theoretically and defined in its architecture only. As a consequence, a complete exercise of compensating the geometry error of a real machine was not possible in the project.

The results obtained in the project suggests that this approach is viable and advantageous for evaluating the geometry errors of Cartesian machine tools.

Thus the technical requirements of the project objective, which was to produce equipment and validated methods for evaluating the performance and compensating for the errors of large machine tools (> 50 m³), have been met - the equipment (in prototype form) has been demonstrated in a laboratory and been shown to deliver 6.4 µm accuracy, and the theoretical model of the error mapping approach has been prepared. Due to lack of time caused by COVID-19, the final software implementation was not completed and demonstration on a machine tool was not possible due to lack of available test device.

4.6 Facilitation of the take up of the technology and measurement infrastructure developed in the project by the measurement supply chain, standards developing organisations e.g. ISO/TC 213, and end users e.g. the automotive and aerospace industry, through operation of one or more demonstration activities, in addition to publications, training, and stakeholder interaction.

Whilst some of the project outputs are directly useable by the stakeholders, for example the new hydrogen cyanide frequency data which we expect users of 1.5 µm scanning laser systems to use directly, other items require more publicity and interaction with the community. Although the COVID-19 pandemic caused the project to abandon the plans for a single large-scale multi-partner demonstrator activity hosted at RWTH, several smaller demonstration activities still took place, and several technology take-up and standardization activities were possible. Standardization activities were relatively limited as they have to follow the processes underway in the various standardization committees as the time. Across the organizations dealing with standards in large volume metrology, there was little work ongoing in the committees, however there was a revision of the ISO standard for laser tracker verification, ISO 10360 Part 10 in 2021 and this document now cites work by NPL on laser tracker verification methods (reference 9 in the document). Additionally, staff from INRIM presented work from the LaVA project at three meetings of ISO TC213 WG10 up until the start of the pandemic. These meetings were located at Poznan (09/2018), Geneva (01/2019), and Berlin (09/2019).

The work on the HCN spectroscopy has been drawn to the attention of Discussion Group 11 (https://www.bipm.org/en/committees/cc/ccl/wg/ccl-dg11) of the Consultative Committee for Length (CCL). DG11 is concerned with *Mise en Pratique* lasers (metre realisation) and femtosecond combs. DG11 includes many of the people who will be assessing the HCN data for inclusion in the *Mise en Pratique* for the definition of the metre. DG11 informed the CCL about the HCN work from LaVA at the 2021 meeting of the CCL. The HCN work was also described at the 2021 meeting of the CCL Working Group on Frequency standards (CCL WGFS). Thus the relevant bodies have been notified to expect new HCN data for their consideration. Relevant journal papers on the HCN spectroscopy work have been published (and 3 additional papers are anticipated after the end of the project, one already having been submitted):

- Investigating the use of the hydrogen cyanide (HCN) as an absorption media for laser spectroscopy, *Proc. SPIE* **1097605**, DOI: 10.1117/12.2517761, https://arxiv.org/abs/1905.07272
- Measurement of the Hydrogen Cyanide Absorption Lines' Centers with the Potential for *Mise en Pratique*, *Proc. IEEE*, DOI: 10.1109/EFTF/IFCS52194.2021.9604261 , https://zenodo.org/record/6497486
- Saturated Spectroscopy of HCN, *Proc. IEEE*, DOI: 10.1109/EFTF/IFCS52194.2021.9604272, https://zenodo.org/record/6497501

As well as the papers on the HCN work, additional peer reviewed papers have been published on the other items of research within the project. The formal list of all publications appears at the end of this document, but they are listed here for information as they are part of the delivery of the impact and take-up objective of the project.

- High-Index Glass Ball Retroreflectors for Measuring Lateral Positions, *Sensors*, **19**(5) 1082 (2019) https://doi.org/10.3390/s19051082
- Artifact-free coordinate registration of Large-Scale Metrology Systems, *CIRP Annals*, **68**(1) 503-506 (2019) https://doi.org/10.1016/j.cirp.2019.04.077
- Model-based interfacing of Large-Scale Metrology instruments, *Proc. SPIE,* **11059** (2019) https://doi.org/10.1117/12.2527461 https://arxiv.org/abs/2001.05897
- Assessment of the mechanical errors of a prototype of an optical multilateration system, *Rev. Sci. Instrum.*, **91** 025004 (2020), https://doi.org/10.1063/1.5132933
- Prototype for dual digital traceability of metrology data using X.509 and IOTA, *CIRP Annals*, **69**(1) 449-452 (2020) https://doi.org/10.1016/j.cirp.2020.04.104
- Uncertainty assessment of a prototype of multilateration coordinate measurement system, *Precision Engineering*, **66** 496-506 (2020) https://doi.org/10.1016/j.precisioneng.2020.08.002 , https://hal-cnam.archives-ouvertes.fr/hal-03190544
- Compact differential plane interferometer with in-axis mirror tilt detection, *Optics and Lasers in Engineering*, **141** 106568 (2021) https://doi.org/10.1016/j.optlaseng.2021.106568
- Absolute multilateration-based coordinate measurement system using retroreflecting glass spheres, *Precision Engineering*, **73** 214-227 (2022) https://doi.org/10.1016/j.precisioneng.2021.09.009

- Multilateration with self-calibration: uncertainty assessment, experimental measurements and Monte-Carlo simulations, *Metrology* **2** 241-262 (2022) https://doi.org/10.3390/metrology2020015
- Optimised calibration of machine vision system for close range photogrammetry based on machine learning, *J. King Saud Uni. Accepted Manuscript* (2022), https://doi.org/10.1016/j.jksuci.2022.06.011

Several items of internal and external training in large volume metrology have taken place. Project partners NPL and RWTH have, between them, provided training for end users at the 2018, 2019, 2020 and 2021 CMSC and 3DMC events (some of which had moved to online only), including the preparation of video-based training material and chairing of a workshop ('Leveraging the Benefits of Machine Tool Calibration'). In December 2018, NPL hosted staff from GUM and provided training in large volume metrology services to assist GUM in setting up a new large volume metrology capability at their Warsaw laboratory.

Aside from providing large volume training at conferences, project outputs have also been presented:

- *Investigating the use of the hydrogen cyanide (HCN) as an absorption media for laser spectroscopy*, CPS 2018- The 21st Czech-Polish-Slovak optical conference on wave and quantum aspects of contemporary optics (09/2018).
- *Using HCN as an absorption media for laser spectroscopy*, Laser 58 (10/2018).
- *Acoustic system for average temperature measurement along a short distance*, 3DMC 2019 (11/2019).
- *Evaluation and improvement of localization algorithms based on UWB Pozyx system*, 27th Intl. Conf. on Software, Telecomms and Computer Networks - SoftCOM (09/2019).
- *Assessment of the mechanical uncertainties of a novel and affordable multilateration system*, 3DMC 2019 (11/2019).
- *Artifact-free coordinate registration of Large-Scale Metrology Systems*, CIRP Gen. Assy., Birmingham (06/2019).
- *Model-based interfacing of Large-Scale Metrology instruments*, SPIE Optical Metrology, Munich (06/2019).
- *Ambient air spectroscopy and thermometry for accurate distance measurement*, OIE 2019 (08/2019).
- *Spectroscopy of ambient air and thermometry for distance measurement*, Optics & Photonics Days 2019 (05/2019).
- *Multilateration*, 3DMC 2019 (11/2019).
- *Acoustic thermometry of air*, 3DMC 2019 (11/2019).
- *Fringe pattern of retroreflecting lateral targets*, CIRP STC "P" meeting (08/2019).
- *A prototype high-accuracy, multi-sensory, multi-target coordinate metrology system using frequency scanning interferometry*, ESA Workshop on Videogrammetry & Contactless Deformation Measurements (12/2019).
- *Dimensional metrology in practice*, Enrico Fermi Varenna Summer School on Metrology, Varenna (07/2019).
- *A Metrology approach for camera calibration based on traceable artefact*, euspen's 20th Intl. Conf. (online) (06/2020).
- *Robotic 3D measurement system for large volume part investigation*, 3DMC 2021 (online) (11/2021).
- *Robot characterization based on a multilateration system with retroreflecting spheres n=2 as targets*, 3DMC 2021 (online) (11/2021).

As can be seen, the COVID-19 pandemic limited the possibility of making presentations during much of 2020 and 2021, however some presentations were possible at online conferences. These conferences are important, especially 3DMC and CMSC, as they are attended by much of the intended stakeholder community, including aerospace manufacturing and particle accelerator scientists.

The multi-partner demonstrator activity planned to take place at RWTH was cancelled due to COVID-19 restrictions and replaced by a series of smaller individual demonstrations at partners in order to mitigate against the imposed travel restrictions.

Firstly, RWTH set up a facility to allow automatic reception and storing of data from individual partners' demonstration activities *via* the internet, shared the specification of the data collection interface and worked with partners to implement data collection for several systems. RWTH the acted as a data collection broker, receiving data from instruments, storing it in a formatted manner, and giving a 'dashboard' display of the collected data. The data transmission uses MQTT (https://mqtt.org/) which is a standard messaging protocol for the *Internet of Things*. Specifically, the implementation used the Paho python client which provides a client class with support for MQTT. TEKNIKER produced a C++ implementation of the interface for use with their AGV tracking system. As well as receiving data sent by partners, RWTH set up a data view client in the form of a dashboard where uploaded data could be sorted and viewed. The access *via* https://iot.wzl-mq.rwth-aachen.de/public/dashboards/d/zhqzZuE7k/lava?refresh=1m was tested by several partners. (Other public dashboards of RWTH can also be viewed on the same website). Data was uploaded by NPL, GUM and TEKNIKER (see below for further details of the TEKNIKER Work). As the multiple measuring heads needed for a full FSI system were not ready, instead NPL uploaded *post hoc* data from a calibration job performed using their laser tracker, to simulate FSI data. GUM uploaded live data from a series of environmental sensors (LAB-EL) in

their laser tracker laboratory and worked with RWTH to implement a C++ interface to their Radian tracker. The Unified Device Interface prepared by RWTH is now publicly available: https://git-ce.rwth-aachen.de/wzl-mq-public/soil

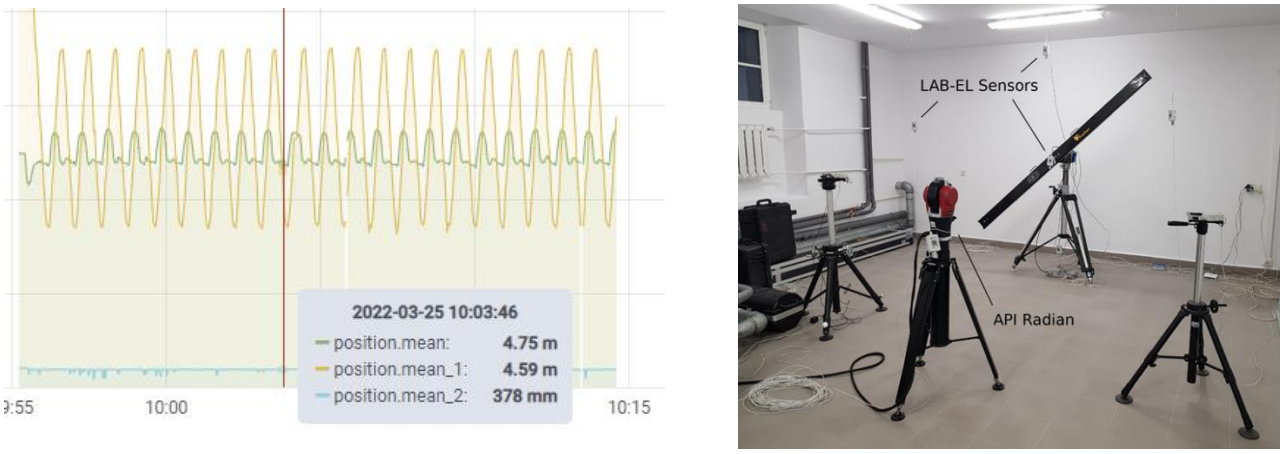

Figure 30 - left: data from the RWTH dashboard captured from the TEKNIKER AGV (as shown in Figure 14); right: sensors in the GUM laser tracker laboratory uploading data to RWTH.

To demonstrate the inter-compatibility of several systems, two sequential bilateral demonstrations were delivered by CNAM working with LNE and RISE. First, the CNAM multilateration system was taken to LNE and coupled to the LNE robotic photogrammetry system. Several glass sphere targets from CNAM were mounted on the photogrammetric scanner made by LNE. The CNAM system was used to track the LNE scanner head in order to determine precisely the pose of the scanner, when moved by the robot. This demonstrates that the working volume of the scanner could be greatly enhanced by mounting it on a large motion system (e.g. an AGV) and having it tracked using the CNAM system. In theory, the measurement volume would then only be limited by the range of the telemetric heads of the CNAM system.

Secondly, in order to prove the uncertainty claim of the CNAM multilateration system, staff from RISE travelled by car to CNAM (Sweden to Paris) and brought their Leica AT960-LR laser tracker. A series of target locations was surveyed first by the CNAM system, and then by the RISE laser tracker. A measurement volume of 6.3 m × 10.3 m × 3.1 m with measurement lines of up to 9.5 m for the laser tracker and 11.6 m for the multilateration system measuring heads, was achieved. A total of 18 target positions were measured by both systems. The results showed that the CNAM uncertainty budget value of between 4.3 µm and 4.7 µm was proven to be correct.

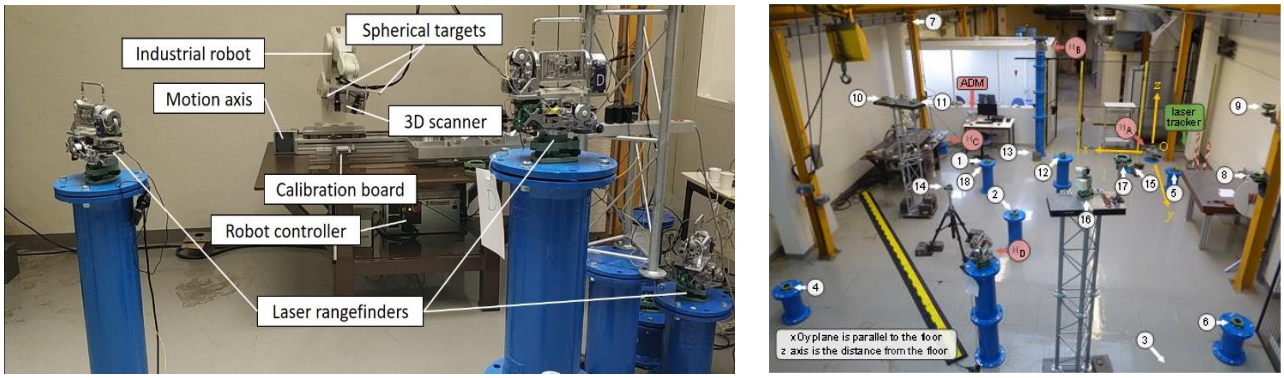

Figure 31 – left: combined LNE photogrammetry system on robot and CNAM multilateration system; right: verification of the CNAM system using the RISE laser tracker.

At TEKNIKER, the low cost 3D position measuring system, which had been developed for the real-time 3D tracking of moving objects in large volumes, was set up on their large shop floor. An autonomously guided vehicle (AGV) was provided with one of the active IR targets developed by TEKINIKER and was tracked by the 3D measuring system. The measuring system had a C++ coded implementation of the Unified Device Interface from RWTH installed, such that the live position data of the AGV was published across the internet to the data collection servers at RWTH. The data shown in Figure 30 is data which was uploaded from the TEKNIKER AGV – one can see the almost constant *Z* coordinate of the target (height above the floor) whilst

the *X* and *Y* coordinates change as the AGV moves around the shop floor. Data was uploaded to RWTH every 1.5 seconds. This dataset encapsulates three entities from the project: the self-illuminated IR targets, the low cost 3D camera system, and the unified device inteface, all working cooperatively in a pseudo demonstrator of AGV positioning on a typical shop floor location.

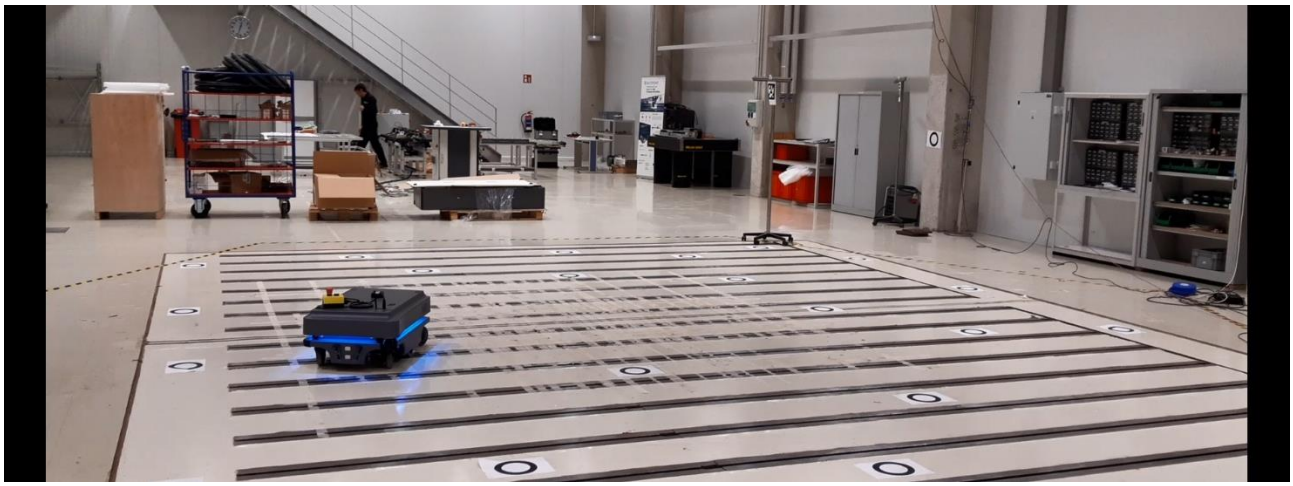

Figure 32 - an AGV at TEKNIKER being tracked using their photogrammetry camera system, with data being uploaded to the RWTH server. Image is a screen shot from a video which will be made available from the project website, http://empir.npl.co.uk/lava/.

Three additional demonstrations took place at VTT, CNAM and INRIM, where they demonstrated the capabilities of their 3 novel thermometer systems, which, unline current sensing based on single point Pt100 sensors, can determine the mean temperature along the beam path for optical measuring instruments such as laser trackers and NPL's FSI system. Air temperature affects the refractive index which causes both wavelength changes (*i.e*. errors in range determination) and, when the air is stratified, beam bending by refractions (*i.e*. pointing errors). The VTT system was deonstrated on a 30 m interferometer bench, where a 10 m length of piping was used to force temperature changes in the ambient air. Their spectroscopic thermometer beam was able to obtain temperatures along the path length with accuracies ranging from 0.2 °C to 0.5 °C over temperatures from 20 °C to 40 °C. A particularly attractive feature of the VTT system is that it does not need calirbating.

Figure 33 - testing of the VTT spectroscopic thermometer along a 30 m bench.

The CNAM system is an acoustic thermometer which uses time of flight data to calculate the refractive index of the air. CNAM performed demonstration measurements of their acoustic thermometer in a laboratory where the temperature could be caried over the range 16.0 °C to 23.5 °C.

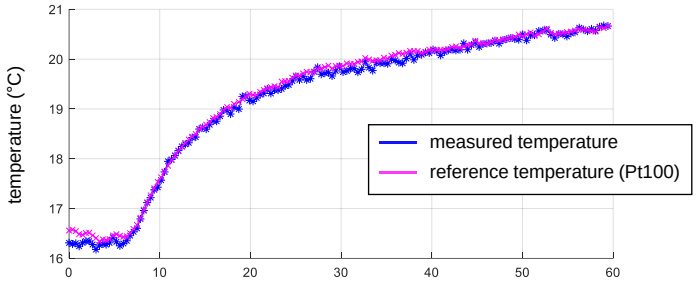

Figure 34 - the CNAM acoustic thermometer operating at a range of 8.99 m and tracking air temperature variation over the period of an hour.

Operating over path lengths up to 10.7 m, CNAM's thermometer produced air temperature data in agreement with the nearby Pt100 sensors to within the combined uncertainty budgets of the two systems, demonstrating temperature measurement uncertainties ranging from 0.09 °C to 0.13 °C with residuals in the range 0.1 °C to 0.2 °C. The system was able to track the change in air temperature over a period of an hour.

The INRIM thermometer was also an acoustic thermometer but used elapsed phase measurement to derive a value for the speed of sound in air, and thus the refractive index. INRIM demonstrated the ability of their system to obtain 0.1 °C uncertainty in the air temperature measurements along the beam. They also demonstrated the ability of using two of their systems mounted one above the other, operating at different frequencies, to measure vertical air temperature gradients with a similar uncertainty. This is important when using 'pointing' systems such as laser trackers as air temperature gradients cause beam bending which leads to incorrect target location (the tracker has to point slightly to the side of the target in order for the beam to hit it, and the erroneous pointing direction is assumed to be the correct one in the polar coordinate system).

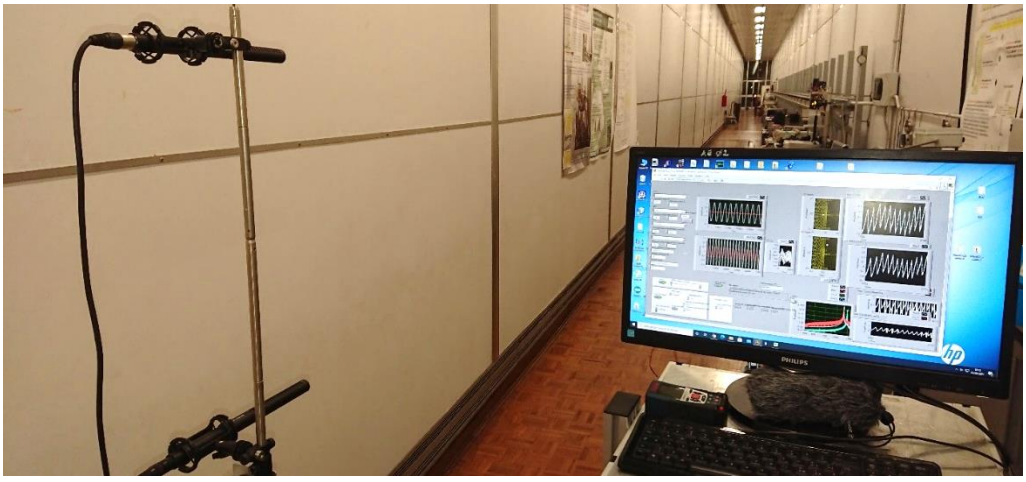

Figure 35 - a pair of INRIM acoustic thermometers being used over a 26 m range, to determine a vertical air temperature gradient.

Further dissemination activities from the project have included three PhD theses:

- Optical thermometry for determining the refractive index of air, Tuomas Helojärvi, Aalto University (2019) https://aaltodoc.aalto.fi/handle/123456789/41644
- Virtual reference frame based on distributed large-scale metrology providing coordinates as a service, Benjamin Montavon, RWTH (2021) https://doi.org/10.18154/RWTH-2021-10238
- Metrologic investigation of mechanical parts using 3-dimensional scanner, Safouane El Ghazouali (submission pending in 2022)

Three direct exploitation/uptake activities have resulted. Firstly, RWTH are in discussion with a Metrology company which has shown interest in implementing the Universal Device Interface. The same company is also considering using NPL's FSI system). Secondly, NPL has been asked to build a copy of its FSI-based system ('OPTIMUM') for the Advanced Machinery and Productivity Institute (AMPI) (https://www.ampi.org.uk/) as part of NPL's contribution to the venture. Finally, NPL has been asked to supply another 'OPTIMUM' system to the Advanced Manufacturing Research Centre in Wales (https://www.amrc.co.uk/facilities/amrc-cymru-wales). All

three outputs show the interest from the end user community in using outputs from the project in their manufacturing and metrology activities. In March 2022 NPL took a measuring head from the OPTIMUM system to demonstrate at AMRC Wales where it was viewed by a number of AMRC's member including Airbus and Electroimpact and the same metrology company that is interested in the Unified Device Interface.

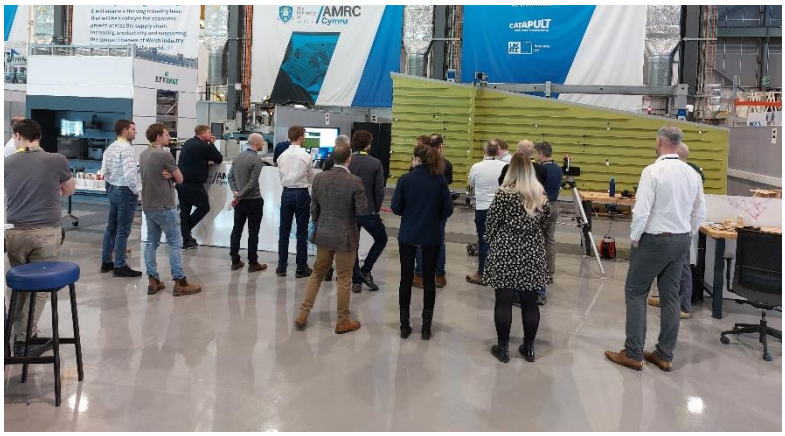

Figure 36 - NPL's OPTIMUM system measuring head being viewed at AMRC Wales in March 2022.

Thus, it can be seen that project outputs are already being taken up by the intended end user community. Further uptake is likely, thus needs of this objective, on ensuring take up of project outputs, have been addressed successfully.

Finally, it should be noted that several of the project partners will continue their work under the follow-on EMPIR project, *DynaMITE* (Dynamic applications of Metrology in Industry of Tomorrow Environments) http://empir.npl.co.uk/dynamite/. Under this project some of the mostly static systems from the LaVA project will be upgraded to cope with dynamic situations (moving targets) ensuring further applications can be targeted.

5 Impact

Direct project outputs

Twelve articles have been published as open access peer-reviewed papers and three others are in preparation for submission after the end of the project. Project partners have presented papers or posters to scientific or mixed audiences at seventeen national or international conferences and workshops and given face-to-face six training sessions (internal training for project partners and training sessions at the two major LVM conferences - Coordinate Metrology Society Conference (CMSC) in the USA and 3D Metrology Conference (3DMC) in the EU). Project partners are co-organisers of 3DMC. One member of staff at partner VTT has submitted his MSc thesis on the spectroscopic thermometry system, another member at RWTH has submitted a PhD thesis on unified interfacing and process modelling, and a third person (from LNE) is about to submit a PhD thesis on work in photogrammetric scanning. The University of Oxford is working on FSI with NPL and the University of South Wales is working with NPL on photonics for the FSI system (both collaborations outside of the LaVA project). One patent has been applied for by participant IK4-TEKNIKER in the subject of spatial tracking of objects.

Impact on industrial and other user communities

Impact on these communities will happen through the use of the project's outputs as metrology enablers for digitisation of European industries manufacturing large items (*e.g*. aerospace, automotive, civil nuclear build). Many organisations are building robotic manufacturing and inspection cells but what is *missing* is the data *traceability*, especially for larger measurands – the robots measure a feature and give a result, but without any estimate of the measurement uncertainty. The Digitally Enabled Supply Chain (DESC) is reliant at its core on valid data and without meta data such as *uncertainty* and *SI traceability routes*, the outputs of these expensive systems are 'images', 'pictures', and estimates – they are not measurements. To facilitate the take-up of the project outputs, the project has undertaken several demonstrator activities and these will be reported in future conference publications.

The Unified Device Interface is already made publicly available (https://git-ce.rwth-aachen.de/wzl-mq-public/soil) including example implementations for three commercial instruments. Discussions are underway

with a metrology company which is interested in implementing the Interface for LVM tools. NPL has received requests from both the AMRC and AMPI organisations to supply them with commercial copies of the FSI-based OPTIMUM system which will use work from the LaVA project (HCN data) and from previous project LUMINAR. The OPTIMUM system will additionally be developed further in the DynaMITE project (http://empir.npl.co.uk/dynamite/) to update it to be able to handle faster-moving targets. There is ongoing interest in OPTIMUM expressed by the aerospace community at the annual 3DMC and CMSC events. The CNAM multilateration system is already being used in the DynaMITE project to provide metrology for a large cable-crane robot in Montpelier, owned by a research organisation. Other outputs such as the robotic photogrammetric scanner from LNE, and the IR-targeted photogrammetry system from TEKNIKER are designed with aerospace manufacturing in mind.

Impact on the metrology and scientific communities

Some project partners' are members of the EURAMET Technical Committee for Length (TC-Length) and Consultative Committee for Length (CCL) at BIPM. The project has helped develop metrology capability at the smaller NMIs – for example GUM has set up and equipped a LVM laboratory and participated in many aspects of the project, gaining experience of research and knowledge of current LVM tools and techniques including submitting data to the end of project data aggregator at RWTH. The inclusion of several external partners has strengthened the interaction between the metrology and non-NMI communities, *e.g.* between NPL and ISI, VTT and MAPVISION, and INRIM and FID. The HCN spectroscopy data is already being used by NPL in its FSI system and other NMIs have stated that they wish to see the data ratified by the CCL and enter the List of *Recommended Values of Standard Frequencies* for realising the metre, published by the BIPM(https://www.bipm.org/en/publications/mises-en-pratique/standard-frequencies), and publications on the HCN data by ISI have identified possible uses in metrology for telecommunications. NPL is working with the BIPM and CCL to make entries in the *Recommended Values of Standard Frequencies* list available for download in machine-readable format for automatic inclusion in FSI-based systems.

Impact on relevant standards

LaVA partners made three inputs to the ISO TC213 technical committee on the subject of laser tracker verification testing and work previously performed by NPL has now been cited in the updated issue of standard ISO 10360 Part 10 on laser trackers. The approach developed by NPL was in response to comments from some end users of this standard that regarded the tests as being too cumbersome to perform on a regular basis. The NPL approach is cited as a way of performing interim testing of laser trackers.

Longer-term economic, social and environmental impacts

The Global Navigation Satellite System (GNSS) was invented with military applications as its *raison d'être*, however it is now known for much wider applications of the technology, from mapping applications and personal navigation in mobile phones, to aircraft landing guidance systems, autonomous vehicles, structure monitoring, machine guidance, geophysics studies, climate monitoring, cadastral surveying and many more. From conversations with end users, it is envisaged that outputs from the project will be enabling technologies for indoor precision navigation/coordinate metrology with a similar broadening of the impact that was experienced by GNSS, and will be joined by the commercialisation of other project outputs feeding into factories *etc*. Thus the longer-term impacts will come from the products that are manufactured in the Digitised Factories of the Future using Industry 4.0 approaches. These will include: lighter weight aircraft with reduced shimming and laminar flow wings; more efficiently manufactured cars and vehicles with eco-friendly design for re{-manufacture, -cycling, -use}; cost effective engineering and assembly of large, expensive, critical components for nuclear new build; better control of aerofoil geometry in wind turbines; better alignment of next-generation science and beamline-based facilities (proton therapy systems); the ability to control fusion energy plant engineering for future ramp-up post *ignition*; and new metrology systems for use in hostile environments (undersea engineering, reactor monitoring; nuclear facility stability evaluation).

6 List of publications

1. A Egidi, A Balsamo, and M Pisani, "High-Index Glass Ball Retroreflectors for Measuring Lateral Positions", *Sensors* **19** 1082 (2019). (DOI: 10.3390/s19051082).

2. M Hošek, Š Řeřucha, L Pravdová, M Čížek, J Hrabina, and O Číp, “Investigating the use of the hydrogen cyanide (HCN) as an absorption media for laser spectroscopy”, *Proc. SPIE* **10976**, 21st Czech-Polish-Slovak Optical Conference on Wave and Quantum Aspects of Contemporary Optics, 1097605 (2018). (arxiv.org/pdf/1905.07272).
3. T Pfeifer, B Montavon, M Peterek, and B Hughes, “Artifact-free coordinate registration of heterogeneous Large-Scale Metrology systems”, *CIRP Annals* **68** (1) (2019). (DOI: 10.1016/j.cirp.2019.04.077).
4. B Montavon and M Peterek, “Model-based interfacing of Large-Scale Metrology instruments”, *Proc. SPIE* **11059** Multimodal Sensing: Technologies and Applications, 110590C (2019). (arxiv.org/abs/2001.05897).
5. J Guillory, D Truong, and J-P Wallerand, “Assessment of the mechanical errors of a prototype of an optical multilateration system”, *Review of Scientific Instruments* **91** 025004 (2020). (DOI: 10.1063/1.5132933).
6. M Peterek and B Montavon, “Prototype for dual digital traceability of metrology data using X.509 and IOTA”, *CIRP Annals* **69** (1) 449-452 (2020). (DOI: 10.1016/j.cirp.2020.04.104).
7. J Guillory, D Truong, and J-P Wallerand, “Uncertainty assessment of a prototype of multilateration coordinate measurement system”, *Precision Engineering* **66** 496-506 (2020). (DOI: 10.1016/j.precisioneng.2020.08.002).
8. Š Řeřucha, M Holá, M Šarbort, J Hrabina, J Oulehla, O Číp, and J Lazar, “Compact differential plane interferometer with in-axis mirror tilt detection”, *Optics and Lasers in Engineering*, **141** 106568. (DOI: 10.1016/j.optlaseng.2021.106568).
9. J Guillory, D Truong, J-P Wallerand, and C Alexandre, "Absolute multilateration-based coordinate measurement system using retroreflecting glass spheres", *Precision Engineering*, **73** 214-227 (2022). (DOI: 10.1016/j.precisioneng.2020.08.002).
10. M Hošek, Š Řeřucha, J Hrabina, M Cizek, and O Číp, " Measurement of the Hydrogen Cyanide Absorption Lines’ Centers with the Potential for Mise en Pratique", *Proc. IEEE*, 2021 Joint Conference of the European Frequency and Time Forum and IEEE International Frequency Control Symposium (EFTF/IFCS) 1-3 (2021).
(DOI: 10.1109/EFTF/IFCS52194.2021.9604261), zenodo.org/record/6497486
11. J Hrabina, M Hošek, Š Řeřucha, L Pravdová, J Lazar, O Číp, and Z Pilát, " Saturated Spectroscopy of HCN", *Proc. IEEE*, 2021 Joint Conference of the European Frequency and Time Forum and IEEE International Frequency Control Symposium (EFTF/IFCS), 1-2 (2021).
(DOI: 10.1109/EFTF/IFCS52194.2021.9604272), zenodo.org/record/6497501
12. J Guillory, D Truong, and J-P Wallerand, "Multilateration with self-calibration: uncertainty assessment, experimental measurements and Monte-Carlo simulations", *Metrology* **2**(2) 241-262 (2022). (DOI: 10.3390/metrology2020015)
13. S El Ghazouli, A Vissiere, L-F Lafon, M-L Bouazizi, H Nouira, “Optimised calibration of machine vision system for close range photogrammetry based on machine learning”, Accepted Publication *J. King Saud University – Comp. Info. Sci* (2022), (DOI: 10.1016/j.jksuci.2022.06.011)
14. J Hrabina, M Hosek, S Rerucha, M Cizek, Z Pilat, M Zucco, J Lazar, Ondrej Cip, “:Absolute frequencies of H13C14N hydrogen cyanide hyper-fine transitions in 1,5 μm region with saturated spectroscopy and sub-kHz scanning laser, submitted to *Optics Letters*. https://doi.org/10.48550/arXiv.2206.09232